# Gain Characterization of a Hybrid Raman/parametric amplifier and phase characterization of a Semiconductor Optical amplifier

By

Muhammad Ali Ummy

A dissertation submitted to the Graduate Faculty in Electrical Engineering in partial fulfillment of the requirements for the degree of Doctor of Philosophy
The City University of New York
2008

UMI Number: 3296970

UMI Microform 3296970



ProQuest Information and Learning Company
300 North Zeeb Road
P.O. Box 1346
Ann Arbor, MI 48106-1346

This manuscript has been read and accepted for the Graduate Faculty in

Electrical Engineering in satisfaction of the dissertation requirement

for the degree of Doctor of Philosophy.

| | |
|---|---|
| | Roger Dorsinville, Ph.D._____ |
| _____ | _____ |
| Date | Chair of Examining Committee |
| | Mumtaz Kassir, Ph.D._____ |
| _____ | _____ |
| Date | Executive Officer |

Mark Arend , Ph.D. The City College of the City University of New York
Mohamed Ali, Ph.D. The City College of the City University of New York
Nicholas Madamopoulos, Ph.D The City College of the City University of New York
Ardie D. Walser, Ph.D The City College of the City University of New York
Dr. Nolan, Daniel A , Ph.D. Corning Inc, One Riverfront Plaza, New York

_____

Supervisory Committee

THE CITY UNIVERSITY OF NEW YORK

# Abstract


## Gain Characterization of a Hybrid Raman/parametric amplifier and phase characterization of a Semiconductor Optical amplifier

by

**Muhammad Ali Ummy**

Advisor: Roger Dorsinville
Co-Advisor: Mark Arend

We have investigated two different nonlinear processes in a distributed medium, such as, a highly non-linear fiber (HNLF) and have demonstrated that by combining optical fiber parametric amplification with Raman fiber amplification, we could further extend the flat gain bandwidth of a Raman fiber amplifier. The parametric process enabled an increase in gain bandwidth by extending the gain region to the longer wavelength side of the Raman gain. Two different configurations of the amplifier were investigated, and their gains and bit error performances were characterized. A gain of about 14-15 dB, with a gain flatness of 5-6 dB was observed in both configurations. In the Raman gain region (1545nm-1570nm) there was a negligible power penalty for both configurations, whereas a 1dB to 3dB power penalty is observed in the parametric gain region (1575nm to 1590nm).

We have also demonstrated an experimental methodology to characterize the nonlinear phase of a semiconductor optical amplifier (SOA) as a function of input intensity. The experimental setup was based on an asymmetric Sagnac interferometer and was carried out at three different gain levels by setting the drive current of the SOA to 170mA,

190mA and 200mA  At low input power it was noticed that the signal experienced very small phase change, irrespective of the gain setting of the SOA.  However, as the power increased the phase curves began to diverge.  It was observed that for values of the input signal power beyond 0.001 W, the slopes of the curves became steeper as the gain of the SOA increased  This implied that in order to achieve a large phase shift at low input signal power, the gain level of the SOA must be set to a higher value.

# Acknowledgements

I would like to acknowledge many people for helping me during my doctoral work. I would especially like to thank my advisor, Professor Roger Dorsinville, for his generous time and commitment. Throughout my doctoral work he encouraged me to develop independent thinking and research skills. He continually stimulated my analytical thinking and greatly assisted me with scientific writing. He not only taught me how to do scientific research but also taught me how to think coherently and write coherently. I am also grateful to him for leading me into the exciting field of nonlinear fiber optics. I am thankful to him for his valuable discussions and suggestions.

I am grateful for the assistance, generosity, and advice I received from Professor Mark Arend and Professor Barry Gross. I would like to thank them for the stimulating discussions and answering my questions about laboratory equipment.

I would like to thank Arie Shahar and Eldan Halberthal from Premaluci, Inc.
for providing the SOA. I am grateful to them for taking time to build the controller for the SOA. I am extremely grateful to them for donating both the SOA and the controller to City College of New York

I'd like to thank my family. My father, who is a constant advocator of higher learning, encouraged me and supported me to this day and I thank him for that. I'm grateful to my sisters for their encouragement and enthusiasm. I'm especially grateful to my dear wife for her patience and for helping me keep my life in proper perspective and balance. Without her support and help, it would be impossible for me to come this far.

## Table of Contents

## A. Gain Characterization

**List of Figures** **Figure Page**

# Chapter 1

## 1.1 Historical Review of Previous Work

### A. Hybrid Raman and Parametric Amplification

Two decades ago, the invention of erbium-doped fiber amplifiers (EDFAs) temporarily supplanted ongoing research on fiber Raman amplifiers (FRAs) and Optical parametric amplifiers (OPAs). However, due to the recent availability of high-power compact pump lasers, there has been renewed interest in FRAs and OPAs. We have exploited both of these nonlinear processes to develop a hybrid (FRA/OPA) wide bandwidth all-optical amplifier.

Raman amplifiers have attracted huge attention in recent years as the enabling technology for future long-haul, high-capacity optical communication systems. This is due to the fact that any wavelength within the transparency window of an optical fiber can be amplified by simply adjusting the pump wavelength [1]. This technology has been demonstrated to increase transmission capacity and span length in WDM transmission [2, 3]. In typical applications for transmission systems, FRAs showed superior performance, such as ultra-wide bandwidth, low noise, and suppressed nonlinearities. Discrete Raman amplifiers, using dispersion-compensating fiber (DCF) or highly nonlinear fiber (HNLF), have also been shown to have good noise performance [4, 5] and better signal power budget.

On the other hand, optical parametric amplifiers utilize highly efficient four-wave mixing in an optical fiber, which requires phase matching between the optical signal and the optical pump [6]. One can obtain a bandwidth as large as 200 nm [7] and a gain as high as 49dB [8] by proper design of HNLF.

The increase in demand for larger bandwidth, lower noise figure and lower gain-ripple makes both RFAs and OPAs more attractive than traditional Erbium Doped Fiber Amplifiers (EDFAs) [9]. EDFAs are only limited to ~40nm bandwidth around 1545nm for a single amplifier, and to ~80nm bandwidth around 1565 nm for a multiple stage amplifier. Several studies indicate that, compared to the conventional EDFA, Raman-assisted EDFAs with a hybrid configuration yield lower noise figure (NF) and optical signal-to-noise ratio in long-haul transmission. For example, Seo *et al.* [10] demonstrated that a flat gain characteristic over the entire C and L bands could be achieved by using a Raman/EDFA hybrid amplifier, where C-band amplification was accomplished by direct transitions of Er ions, and L-band amplification was achieved by stimulated Raman scattering (SRS). Kurosawa *et al*. also demonstrated another type of single-pump hybrid amplifier (called Raman-assisted EDFA) to obtain both high pump efficiency and low noise performance [11]. However, with these hybrid configurations, bandwidth is still restricted by the Er ion states.

To enable RFAs to achieve ultra-wide bandwidth, many pumps at different wavelengths are necessary. However, many pump lasers work far below their maximum power to achieve a small gain variation and lower noise figure. Another problem associated with the RFA design is the well-known quandary of pump interactions. The pumps interact with each other by drawing energy from one pump to another. Gain

fluctuation and accompanied noise of individual amplifiers will be multiplied when the number of pumps increases [12].

RFAs and hybrid EDFA/RFA configurations have been widely used to achieve wide bandwidth amplification. However, the combined effect of Raman scattering and parametric amplification has received less attention. In optical fibers, E. Golovchenko *et al.* [13] have examined the phase mismatch parametric gain and have demonstrated that the gain depends strongly on the real part of the complex Raman susceptibility. More recently, Hsieh *et al.* [14] have examined the effect of the frequency detuning between the signal and the pump. Also, Joao *et al*. [15] characterized, both experimentally and theoretically, a Raman-enhanced parametric amplifier. Their focus was on gain enhancement effects, and on the coupling between the two nonlinear processes within a bandwidth where both processes showed strong amplification in a highly nonlinear fiber. They reported a 10dB gain enhancement in the S-band and a net 10dB conversion efficiency [15-18]. However, not much experimental work has been done to develop a wide-band hybrid amplifier by combining optical parametric amplification with Raman amplification.

**B. Non-linear Phase Characterization**

Semiconductor optical amplifiers (SOAs) have been extensively used in making optical switches, wavelength conversion [25], threshold devices and many other optical applications [26-29]. Optical logic gate operations were also performed by using a SOA placed in an asymmetric Mach-Zehnder interferometer. These devices exploited the ultra fast nonlinearities of a SOA and phase change that occurs when the signal passed through

the SOA [30-32]. Many models and experiments were designed to characterize the gain and the nonlinear polarization rotation of a SOA [34], but not much experimental work has been done for the phase characterization [35-36]. we will demonstrate an experimental methodology to characterize the phase as a function of input power to the SOA. This will be carried out at three different gain levels by setting the drive current of the SOA to 170mA, 190mA and 200mA.

## 1.2 **Thesis Objective**

The objective of this thesis is of two folds:

a) In the first half of my thesis we will explore the theories that govern the two non-linear processes i.e. Stimulated Raman Scattering and parametric (Four Wave Mixing) in a highly non-linear fiber (HNLF). These theories will then be used to develop a mathematical model in order to examine the impact on the gain profiles of the amplifier when the Raman and parametric processes either occur separately or jointly. We will then compare the theoretical results with the experimental data. We will investigate two different configurations of the amplifier, Tandem and Unison, and finally, we will characterize their gains and bit error performances.

b) In the second half of my thesis we will develop unique experimental methodology to characterize the phase as a function of input power to the Semiconductor Optical Amplifier (SOA). This will be carried out at three different gain levels by setting the drive current of the SOA to 170mA, 190mA and 200mA.

# Chapter 2

## 2.1 Understanding Nonlinear Optics

Nonlinear optics deals mainly with various new optical effects and novel phenomena arising from the interactions of intense coherent optical radiation with mater. A light wave consists of electric and magnetic fields varying sinusoidally at high frequencies. When light propagates through matter it induces motion of the charged particles that constitute the material. In a dielectric medium the charges are bound together and will start to oscillate in the applied electric field; they form oscillating electric dipoles. The contribution from the magnetic field part of the light and from electric quadrupoles is much weaker and is usually neglected. This is called the electricdipole approximation. The oscillating dipoles add up to a macroscopic polarization $P$ which is used to describe the response of the material. For low light intensities, i.e. small amplitudes of the electric field $E$, the charges can follow the field almost exactly and the relationship between $E$ and $P$ is essentially linear. For larger amplitudes the motion of the particles will be distorted and nonlinear terms will become important. The origin of nonlinear optics can be uncovered by recalling Maxwell's equations [37-38], which are a set of laws governing light-matter interaction.

$$\nabla \cdot D = \rho, \qquad (2.1.1)$$

$$\nabla \cdot B = 0, \qquad (2.1.2)$$

$$\nabla \times E = -\frac{\partial B}{\partial t}, \qquad (2.1.3)$$

$$\nabla \times H = J + \frac{\partial D}{\partial t}, \qquad (2.1.4)$$

where D and B are electric and magnetic flux densities, E and H are electric and magnetic field vectors, r is the charge density, and J is the current density vector. The electric and magnetic flux densities, D and B, are related to the electric and magnetic field vectors, respectively, as follows:

$$D = \varepsilon_0 E + P, \qquad (2.1.5)$$

$$B = \mu_0 H + M, \qquad (2.1.6)$$

where ε0 is the vacuum permittivity and μ0 is vacuum permeability. The induced electric and magnetic polarizations P and M account for the material response. The equation that describes the propagation of the electric field can be written in terms of a single, second-order, partial differential equation known as the electromagnetic wave equation. First, taking the curl of Eq. (2.1.3) and using Eqs. (2.1.5) and (2.1.6) we obtain

$$\nabla \times \nabla \times E = -\frac{\partial(\nabla \times B)}{\partial t} = -\mu_0 \varepsilon_0 \frac{\partial^2 E}{\partial t^2} - \mu_0 \frac{\partial^2 P}{\partial t^2} - \mu_0 \frac{\partial J}{\partial t} - \frac{\partial(\nabla \times M)}{\partial t}. \qquad (2.1.7)$$

As fibers do not typically contain free charges, (ρ = 0 and J = 0) and have a nonmagnetic nature, the last two terms in Eq. (2.1.7) can be dropped. Left-hand side of the equation can be simplified through the identity

$$\nabla \times \nabla \times \boldsymbol{E} = \nabla(\nabla \cdot \boldsymbol{E}) - \nabla^2 \boldsymbol{E} = -\nabla^2 \boldsymbol{E}, \tag{2.1.8}$$

where Eq. (2.1.1) is used in the last step. With these simplifications Eq. (2.1.8) becomes

$$\nabla^2 \boldsymbol{E} - \frac{1}{c^2}\frac{\partial^2 \boldsymbol{E}}{\partial t^2} = \frac{\varepsilon_0}{c^2}\frac{\partial^2 \boldsymbol{P}}{\partial t^2}, \tag{2.1.9}$$

where $\frac{\partial^2 P}{\partial t^2}$ is the induced polarization term. In case of nonlinear manifestations, the polarization vector contains both a linear and a nonlinear contribution of the material. Provided that these new nonlinear terms are still small compared to the linear one, we can expand the polarization vector *P* in a power series in *E*:

$$P(t) = P^{(1)}(t) + P^{(2)}(t) + P^{(3)}(t) + P^{(4)}(t) + \ldots \tag{2.1.10}$$

$$\boldsymbol{P} = \varepsilon_0 \left( \chi^{(1)} \boldsymbol{E} + \chi^{(2)} \boldsymbol{E}^2 + \chi^{(3)} \boldsymbol{E}^3 + \chi^{(4)} \boldsymbol{E}^4 \ldots \right) \tag{2.1.11}$$

Here $\chi^{1}$ is the *linear susceptibility* of the medium, often called the polarizibility and is related to the linear refractive index n by $n^2 = 1 + \chi^{(1)}$. The quantities $\chi^{(2)}, \chi^{(3)}, \ldots$ are the *nonlinear susceptibilities* and they describe the nonlinear-optical properties of the medium.

It is worth mentioning here that even-order nonlinear susceptibilities can not exist in a material with inversion symmetry (Centro-symmetric material). For example, in many isotropic media such as glasses, liquids and gasses, there can be no even powers of the field in the expansion of the polarization for symmetry reasons. The lowest-order nonlinearity is then the cubic term in Eq. (2.1.11).

The importance of the induced polarization can be understood from the fact that any oscillating dipole also emits radiation, at the frequency of oscillation, and thus modifies the optical field that induced the polarization. To demonstrate some of the many nonlinear phenomena that can occur, consider the following incoming field:

$$E(t) = E_1 e^{-i\omega_1 t} + E_2 e^{-i\omega_2 t} + c.c. \qquad (2.1.12)$$

the second-order nonlinear response is given by

$$P^{(2)}(t) = \chi^{(2)}[E_1^2 e^{-2i\omega_1 t} + E_2^2 e^{-2i\omega_2 t} + 2E_1 E_2 e^{-i(\omega_1+\omega_2)t} + 2E_1 E_2^* e^{-i(\omega_1-\omega_2)t} + c.c.] + 2\chi^{(2)}[E_1 E_1^* + E_2 E_2^*] \qquad (2.1.13)$$

Within this expression, it's easy to see various manifestations. The terms in $2\omega_i$ account for *second harmonic generation*; the terms in $\omega_i \pm \omega_2$ are related to the *sum and difference frequency generation*; and the terms independent of $\omega$ (static $E$ fields) are responsible for optical rectification. Connected to this latter effect, is the electro-optic effect where a static field modifies the optical properties of the medium. Most generally, the quadratic term involves the mixing of three different fields (it multiplies two fields to generate a third). This term is thus used for Optical Parametric Conversion by three-wave mixing. In the next chapter we examine the nonlinear four wave mixing in detail.

## 2.2. Basic Properties of FWM

Physically, two photons at the original frequencies are scattered elastically into two new photons at frequencies $\omega_3$ and $\omega_4$ as shown in Fig. 2.2.1.

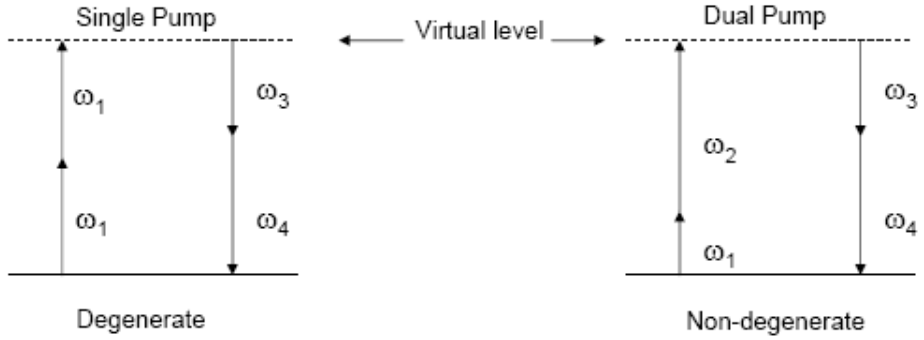


Figure 2.2.1 Degenerate and nondegenerate FWM process depicted on an energy level diagram.

The total energy and momentum of the original two photons are conserved during FWM. Noting that photon energy and momentum are $\hbar\omega$ and $\hbar\beta$, respectively, for an optical field of frequency $\omega$ propagating with the propagation constant $\beta$, the conservation relations takes the form:

$$\omega_1 + \omega_2 = \omega_3 + \omega_4, \tag{2.2.1}$$

$$\beta(\omega_1) + \beta(\omega_2) = \beta(\omega_3) + \beta(\omega_4), \tag{2.2.2}$$

Only the magnitude of wave vectors appears in Eq. (2.2.1), because all four waves propagate along the same direction in single-mode fibers. A question that must be answered is what determines the frequencies $\omega_3$ and $\omega_4$ during the FWM process. If only

the pump beams are incident on an optical fiber, the new waves grow from noise and their frequencies are determined by the phase matching condition through spontaneous FWM. In practice, the efficiency of the FWM process is enhanced by seeding it. Seeding is accomplished by launching a signal wave at the frequency $\omega_4$. The probability of creating photons at the frequency $\omega_4$ depends on how many photons at $\omega_3$ already exist inside the fiber. As a result, the FWM process is stimulated, and new photons at $\omega_3$ and $\omega_4$ are created with an exponential growth rate, provided the phase-matching condition is nearly satisfied. It is common to refer to the fourth wave at the frequency w4 as the idler wave, following the terminology used in the microwave literature. It is not obligatory to launch two separate pump beams for FWM to occur. The same process can occur even when the two pump photons have the same frequency (degenerate FWM). The general case of two independent pump beams is called non-degenerate FWM.

## 2.3 Third-order Nonlinear Response

The next step is to incorporate the effect of third-order nonlinearity into Eq. (2.1.9).

To do that, a few approximations and simplifications are needed. The first of these simplifications comes from the assumption that the field is quasi-monochromatic. This assumption, also known as the slowly-varying envelope approximation, is valid whenever the spectral spread $\Delta\omega$ of the field is much smaller than the central frequency $\omega_0$ of the spectrum. This approximation remains valid until the width of the field envelope reduces to below a few optical cycles. The second simplification is due to the fact that nonlinear induced polarization is much smaller than the linear induced polarization and it does not affect the transverse field distribution to the first order. Finally, it is assumed that the dipole approximation is valid and the material response is local. With these assumptions in mind, the electric field can be written as[38-40]

$$E(r,t) = \frac{1}{2}[\hat{x}E_x(r,t) + \hat{y}E_y(r,t)]\exp(-i\omega_0 t) + \text{c.c.}, \qquad (2.3.1)$$

where ˆ x and ˆ y are unit vectors, Ex and Ey are the two polarization components of the slowly varying envelope in the linear basis. The optical field is propagating along the z axis with an unchanging transverse profile. The material response of the fiber can also be separated into its slowly varying envelope and its rapidly oscillating carrier frequency in a similar way as

$$P(r,t) = \frac{1}{2}\{\hat{x}[P_{Lx}(r,t) + P_{NLx}(r,t)] + \hat{y}[P_{Ly}(r,t) + P_{NLy}(r,t)]\}\exp(-i\omega_0 t) + \text{c.c.} \tag{2.3.2}$$

Using Eqs. (2.1.11), (2.1.13), (2.2.1) and (2.2.2), the expression for the slowly varying envelope of the induced polarization becomes

$$P_{Li}(r,t) = \varepsilon_0 \int_{-\infty}^{\infty} \sum_j \chi_{ij}^{(1)}(t-t')E_j(r,t')\exp[i\omega_0(t-t')]\,dt', \tag{2.3.3}$$

$$P_{NLi}(r,t) = \varepsilon_0 \frac{3}{4} \sum_{j,k,l} \chi_{ijkl}^{(3)} E_j(r,t)E_k(r,t)E_l(r,t)^*, \tag{2.3.4}$$

where i, j, k, and l stand for x or y. In deriving Eq. (2.3.4), the induced nonlinear polarization at the third harmonic of the electric field is ignored since this process rarely satisfies the phase-matching condition to have an appreciable contribution. The factor of three in the expression is the number of ways the three fields can mix up to create a response at the carrier frequency.

In an isotropic medium such as an optical fiber, the elements of the nonlinear susceptibility tensor cannot be completely independent but must satisfy several relations imposed by the material symmetry. As a result, the number of independent elements of $\chi^{(3)}$ reduce to three and they satisfy the following relation

$$\chi_{ijkl}^{(3)} = \chi_{xxyy}^{(3)}\delta_{ij}\delta_{kl} + \chi_{xyxy}^{(3)}\delta_{ik}\delta_{jl} + \chi_{xyyx}^{(3)}\delta_{il}\delta_{jk}, \tag{2.3.5}$$

where $\delta_{ij}$ is the Kronecker delta function. Using Eq. (2.3.5), nonlinear part of the induced polarization can be written as

$$P_{NLi} = \frac{3\varepsilon_0}{4} \sum_j \left( \chi_{xxyy}^{(3)} E_i E_j E_j^* + \chi_{xyxy}^{(3)} E_j E_i E_j^* + \chi_{xyyx}^{(3)} E_j E_j E_i^* \right). \tag{2.3.6}$$

The relative contributions of the three independent terms are determined by the physical origin of the nonlinear process. In fibers and other materials where the nonlinearity is mainly of electronic origin, all of the three independent terms contribute equally.

Finally, using Eq. (2.3.6) they can be expressed in terms of the single parameter $\chi^{(3)}_{xxxx}$

$$\frac{1}{3}\chi^{(3)}_{xxxx} = \chi^{(3)}_{xxyy} = \chi^{(3)}_{xyxy} = \chi^{(3)}_{xyyx}. \tag{2.3.7}$$

Equation (2.3.5) can be simplified even further using Eq. (2.3.7) to become

$$P_{NLi} = \frac{\varepsilon_0 \chi^{(3)}_{xxxx}}{4} \sum_j \left( E_i E_j E_j^* + E_j E_i E_j^* + E_j E_j E_i^* \right) \tag{2.3.8}$$

The explicit forms of nonlinear induced polarization along the x- and y-axis becomes

$$P_{NLx} = \frac{3\,\varepsilon_0 \chi^{(3)}_{xxxx}}{4} \left[ \left( |E_x|^2 + \frac{2}{3}|E_y|^2 \right) E_x + \frac{1}{3} E_x^* E_y^2 \right], \tag{2.3.9}$$

$$P_{NLy} = \frac{3\,\varepsilon_0 \chi^{(3)}_{xxxx}}{4} \left[ \left( |E_y|^2 + \frac{2}{3}|E_x|^2 \right) E_y + \frac{1}{3} E_y^* E_x^2 \right]. \tag{2.3.10}$$

The equations governing the evolution and interaction of the two polarization components of the field can be written in a compact form in the Jones space. In this notation, complex valued electric field components are represented by the elements of a vector as shown in the following example:

$$|E(r,t)\rangle = \begin{pmatrix} E_x(r,t) \\ E_y(r,t) \end{pmatrix}, \qquad |P(r,t)\rangle = \begin{pmatrix} P_x(r,t) \\ P_y(r,t) \end{pmatrix}. \tag{2.3.11}$$

With this notation, Eqs. (2.3.9) and (2.3.10) can be written in a simpler form as

$$|P_{NL}\rangle = \varepsilon_0 \overleftrightarrow{\varepsilon}_{NL} |E\rangle, \qquad \overleftrightarrow{\varepsilon}_{NL} = \frac{3\chi^{(3)}_{xxxx}}{4} \begin{pmatrix} |E_x|^2 + \frac{2}{3}|E_y|^2 & \frac{1}{3}E_x^* E_y \\ \frac{1}{3}E_y^* E_x & |E_y|^2 + \frac{2}{3}|E_x|^2 \end{pmatrix} \tag{2.3.12}$$

Complex valued 2×2 matrices such as the one shown in Eq. (2.3.12) can also be represented in a simpler form by introducing the Pauli matrices defined as

$$\sigma_1 = \begin{pmatrix} 1 & 0 \\ 0 & -1 \end{pmatrix} \qquad \sigma_2 = \begin{pmatrix} 0 & 1 \\ 1 & 0 \end{pmatrix} \qquad \sigma_3 = \begin{pmatrix} 0 & -i \\ i & 0 \end{pmatrix}. \tag{2.3.13}$$

Together with the identity matrix $\sigma_0$ these matrices form a complete set in the sense that any 2×2 matrix can be written as a linear combination of them, for example

$$\overleftrightarrow{\varepsilon}_{NL} = \frac{3\chi^{(3)}_{xxxx}}{4} \left[ \frac{5}{6}\langle E|E\rangle \sigma_0 + \frac{1}{6}\langle E|\sigma_1|E\rangle \sigma_1 + \frac{1}{6}\langle E|\sigma_2|E\rangle \sigma_2 - \frac{1}{6}\langle E|\sigma_3|E\rangle \sigma_3 \right] \tag{2.3.14}$$

To make the notation more compact, one can show that

$$|P_{NL}\rangle = (3\varepsilon_0 \chi^{(3)}_{xxxx}/4)\Gamma |E(r,t)\rangle \tag{2.3.15}$$

where

$$\mathbf{\Gamma} = \langle E|E\rangle\sigma_0 - \frac{1}{3}\langle E|\sigma_3|E\rangle\sigma_3. \tag{2.3.16}$$

Written this way, the two contributions to the nonlinear response of the material can be identified. The first term on the left-hand side of Eq. (2.3.16), depends only on the total power of the field and it affects both polarization components of the field equally. Therefore contribution of this term is said to be isotropic. The second term is a traceless matrix and it leads to what is known as the nonlinear birefringence. When the electric field is linearly or circularly polarized, the second term in Eq. (2.3.16) vanishes and it does not experience nonlinear birefringence. In contrast, any elliptically polarized field experiences an effective birefringence and propagates in a way that transfers the energy back and forth between the two polarization components.

## 2.4 Vectorial FWM Equations

The vectorial nonlinear Schrödinger equation can be used to describe various nonlinear processes that take place in a FOPA. An important nonlinear process is four-wave mixing (FWM); it allows power transfer from one or more strong pump fields to the so-called signal and idler fields. Launching only the strong pump fields leads to spontaneous parametric scattering. The process becomes stimulated when a weak signal field is launched together with the pump. As a result, the signal field is amplified and at the same time the idler is created such that the four fields satisfy the energy conservation requirement

$$\omega_1 + \omega_2 = \omega_3 + \omega_4, \tag{2.4.1}$$

where w1, w2, w3 and w4 are the frequencies for the two pumps, signal and idler respectively. If only a single pump is used, energy conservation requirement becomes

$$2\omega_1 = \omega_3 + \omega_4. \tag{2.4.2}$$

As the four interacting fields are spectrally distinct, it is possible to obtain a separate equation for each field that explicitly shows the nonlinear interaction among them. To do this, the field is assumed to have the following form

$$|A(z,t)\rangle = \sum_{m=1}^{4} |A_m(z,t)\rangle \exp\{-i\beta(\omega_0)z - i(\omega_m - \omega_0)t\}. \tag{2.4.3}$$

Substituting Eq. (2.4.3) into propagation equation and separating different frequency components we obtain

$$\frac{\partial|A_j\rangle}{\partial z} = \mathscr{L}(\omega_j)|A_j\rangle + i\gamma\Big\{\langle A_j|A_j\rangle - \frac{1}{3}\langle A_j|\boldsymbol{\sigma_3}|A_j\rangle\boldsymbol{\sigma_3} + \sum_{m\neq j}^{4}\Big[\langle A_m|A_m\rangle + |A_m\rangle\langle A_m| - \frac{1}{3}\Big(\langle A_m|\boldsymbol{\sigma_3}|A_m\rangle + \boldsymbol{\sigma_3}|A_m\rangle\langle A_m|\Big)\boldsymbol{\sigma_3}\Big]\Big\}|A_j\rangle + i\gamma\Big[|A_3\rangle\langle A_4^*| + |A_4\rangle\langle A_3^*| - \frac{\boldsymbol{\sigma_3}}{3}\Big(|A_3\rangle\langle A_4^*| + |A_4\rangle\langle A_3^*|\Big)\boldsymbol{\sigma_3}\Big]|A_{3-j}^*\rangle e^{-i\Delta\beta z}, \tag{2.4.4}$$

$$\frac{\partial|A_k\rangle}{\partial z} = \mathscr{L}(\omega_k)|A_k\rangle + i\gamma\Big\{\langle A_k|A_k\rangle - \frac{1}{3}\langle A_k|\boldsymbol{\sigma_3}|A_k\rangle\boldsymbol{\sigma_3} + \sum_{m\neq k}^{4}\Big[\langle A_m|A_m\rangle + |A_m\rangle\langle A_m| - \frac{1}{3}\Big(\langle A_m|\boldsymbol{\sigma_3}|A_m\rangle + \boldsymbol{\sigma_3}|A_m\rangle\langle A_m|\Big)\boldsymbol{\sigma_3}\Big]\Big\}|A_k\rangle + i\gamma\Big[|A_1\rangle\langle A_2^*| + |A_2\rangle\langle A_1^*| - \frac{\boldsymbol{\sigma_3}}{3}\Big(|A_1\rangle\langle A_2^*| + |A_2\rangle\langle A_1^*|\Big)\boldsymbol{\sigma_3}\Big]|A_{7-k}^*\rangle e^{i\Delta\beta z}, \tag{2.4.5}$$

where, j = 1 or 2, k = 3 or 4, m runs from 1 to 4, $\gamma$ is the nonlinearity which is derived in chapter 3 and $\Delta\beta$ is the wave-vector mismatch given by

$$\Delta\beta = \beta(\omega_3) + \beta(\omega_4) - \beta(\omega_1) - \beta(\omega_2). \tag{2.4.6}$$

The linear operator $L(\omega_m)$ governs the evolution of the fields in the absence of nonlinearity and is given by

$$\mathscr{L}(\omega_m) = -\frac{\alpha}{2} + i\left(\vec{b}_0(\omega_m) + i\vec{b}_1(\omega_m)\frac{\partial}{\partial t}\right)\cdot\vec{\boldsymbol{\sigma}} + \beta(\omega_m) - \beta_1(\omega_m)\frac{\partial}{\partial t} - i\frac{\beta_2(\omega_m)}{2}\frac{\partial^2}{\partial t^2}. \tag{2.4.7}$$

In Eqs. (2.4.4) and (2.4.5) the terms containing the nonlinearity coefficient g show explicitly the nonlinear interactions among the fields. The first two terms are the SPM terms since they depend only on the field itself, and their only effect is to modify the phase of the field. Similarly, the terms gathered within the summation symbol only affect the phase of the field. Since these terms only consist of other fields, they are called the cross-phase modulation (XPM) terms. The last four terms are responsible for the FWM process. Unlike the SPM and XPM terms, the FWM terms are not purely imaginary; as a result, FWM can lead to power exchange among the fields. The efficiency of the energy exchange depends on the wave-vector mismatch Db as well as on how strong the fields are. Equations (2.4.4) and (2.4.5) describe the general case where the signal and idler fields can be as strong as the pumps. In fact, these equations are symmetric in the sense that subscripts 1 and 2 can be exchanged freely with 3 and 4, which also shows that energy flow can be from pumps to the signal and idler or vice versa. In practice, pump fields are much stronger than the signal and idler fields. Assuming weak signal and idler fields, we can drop those terms that are proportional to signal or idler amplitudes in Eq. (2.4.4) and linearize Eq. (2.4.5) in terms of the signal and idler fields as follows

$$\frac{\partial |A_1\rangle}{\partial z} = \mathscr{L}(\omega_1)|A_1\rangle + i\gamma\Big[\langle A_1|A_1\rangle + \langle A_2|A_2\rangle + |A_2\rangle\langle A_2| - \frac{1}{3}\Big(\langle A_1|\boldsymbol{\sigma_3}|A_1\rangle + \langle A_2|\boldsymbol{\sigma_3}|A_2\rangle + \boldsymbol{\sigma_3}|A_2\rangle\langle A_2|\Big)\boldsymbol{\sigma_3}\Big]|A_1\rangle, \tag{2.4.8}$$

$$\frac{\partial|A_3\rangle}{\partial z} = \mathscr{L}(\omega_3)|A_3\rangle + i\gamma\sum_{m=1}^{2}\Big[\langle A_m|A_m\rangle + |A_m\rangle\langle A_m| - \frac{1}{3}\Big(\langle A_m|\boldsymbol{\sigma_3}|A_m\rangle + \boldsymbol{\sigma_3}|A_m\rangle\langle A_m|\Big)\boldsymbol{\sigma_3}\Big]|A_3\rangle + i\gamma\Big[|A_1\rangle\langle A_2^*| + |A_2\rangle\langle A_1^*| - \frac{\boldsymbol{\sigma_3}}{3}\Big(|A_1\rangle\langle A_2^*| + |A_2\rangle\langle A_1^*|\Big)\boldsymbol{\sigma_3}\Big]|A_4^*\rangle e^{i\Delta\beta z}, \tag{2.4.9}$$

where equations for the second pump and the idler can be obtained by exchanging the subscript 1 with 2 in Eq. (2.4.8) and 3 with 4 in Eq. (2.4.9). Note also that as a result of neglecting terms that are proportional to signal and idler fields in Eq. (2.4.8), pump fields remain undeleted. In many applications, continuous-wave (CW) or quasi-CW pumps are used. In this case, Eqs. (2.4.8) and (2.4.9) can be simplified even further since pumps retain their temporal profile. The change in the temporal profile of the pump is negligible as long as fiber is much shorter than the dispersion length L < $L_D$. When the pump fields have a narrow spectral width, and fiber losses are neglected for a relatively short fiber, the terms related to linear propagation of the fields L($w_m$) in Eqs. (2.4.8) and (2.4.9) can be simplified to

$$\mathscr{L}(\omega_m) \approx i\vec{b}_0(\omega_m)\cdot\vec{\boldsymbol{\sigma}}. \tag{2.4.10}$$

With these simplifications, it can be shown easily that pump powers remain unchanged during the propagation:

$$\frac{\partial\langle A_1|A_1\rangle}{\partial z} = \frac{\partial\langle A_2|A_2\rangle}{\partial z} = 0. \tag{2.4.11}$$

However, pump phases and polarizations can still evolve in a complicated manner depending on their initial values. Making use of the fact that pump powers remain constant, and by introducing a change of variables such that

$$|B_1\rangle = \exp\left[i\left(\langle A_1|A_1\rangle + \langle A_2|A_2\rangle\right)z\right]|A_1\rangle, \tag{2.4.12}$$

$$|B_3\rangle = \exp\left[i\left(\langle A_1|A_1\rangle + \langle A_2|A_2\rangle + \frac{\Delta\beta}{2}\right)z\right]|A_3\rangle. \tag{2.4.13}$$

Equations (2.4.8) and (2.4.9) can be written as

$$\frac{d|B_1\rangle}{dz} = i\vec{b}_0(\omega_1)\cdot\vec{\sigma}|B_1\rangle + i\gamma\left[|B_2\rangle\langle B_2| - \frac{1}{3}\left(\langle B_1|\boldsymbol{\sigma_3}|B_1\rangle + \langle B_2|\boldsymbol{\sigma_3}|B_2\rangle + \boldsymbol{\sigma_3}|B_2\rangle\langle B_2|\right)\boldsymbol{\sigma_3}\right]|B_1\rangle, \tag{2.4.14}$$

$$\begin{aligned}\frac{d|B_3\rangle}{dz} = {} & i\vec{b}_0(\omega_3)\cdot\vec{\sigma}|B_1\rangle + i\frac{\Delta\beta}{2}|B_3\rangle \\ & + i\gamma\sum_{m=1}^{2}\left[|B_m\rangle\langle B_m| - \frac{1}{3}\left(\langle B_m|\boldsymbol{\sigma_3}|B_m\rangle + \boldsymbol{\sigma_3}|B_m\rangle\langle B_m|\right)\boldsymbol{\sigma_3}\right]|B_3\rangle \\ & + i\gamma\left[|B_1\rangle\langle B_2^*| + |B_2\rangle\langle B_1^*| - \frac{\boldsymbol{\sigma_3}}{3}\left(|B_1\rangle\langle B_2^*| + |B_2\rangle\langle B_1^*|\right)\boldsymbol{\sigma_3}\right]|B_4^*\rangle.\end{aligned} \tag{2.4.15}$$

Once again, equations for the evolution of the second pump and the idler can be found by exchanging the subscripts 1 by 2 and 3 by 4. The preceding FWM equations are derived for the more general case in which two pumps with distinct frequencies are used. FWM equations in the case of a single pump FOPA can also be derived by the same procedure. These equations can also be obtained from the dual-pump FWM equations (2.4.14) and

(2.4.15) by putting $|A_2\rangle$ = 0, in Eq. (2.4.12) and by replacing both $|A_2\rangle$ and $|A_1\rangle$ by $\frac{|A_1\rangle}{\sqrt{2}}$ in Eq. (2.4.13). The FWM equations Eq. (2.4.3) that includes pump depletion can also be used to get the single pump equations in the same way.

## 2.5 Scalar FWM Equations

Even though Eqs. (2.4.12) and (2.4.13) are linear equations, they do not have a closed form analytical solution since in general pumps undergo a complicated nonlinear polarization rotation depending on their initial SOPs. It is possible to get solutions in the special cases in which pumps retain their SOPs. It is easy to verify from Eq. (2.4.8) that if the fiber has negligible birefringence, and both pumps are either linearly or circularly polarized such that their SOPs are either parallel or orthogonal, then pumps do not undergo nonlinear-polarization rotation. In fact, these four cases are frequently used in practice. Among these four schemes, it is instructive to examine the situation when all fields have the same linear SOP. Assuming that a field with narrower spectral bandwidth is traveling in a fiber with small birefringence and that fiber losses can be neglected, the solution of Eq. (2.4.13) for the non-depleted pumps can be written as follows

$$A_1(z) = A_1(0)\exp(2i\gamma P_2 z) \tag{2.5.1}$$

$$A_2(z) = A_2(0)\exp(2i\lambda P_1 z) \tag{2.5.2}$$

Inserting the solution for the pump fields into Eq. (2.4.13) for the signal and a similar equation for the idler leads to:

$$\frac{dA_3}{dz} = \frac{i}{2}\kappa A_3 + 2i\gamma A_1 A_2 A_4^* \qquad (2.5.3)$$

$$\frac{dA_4}{dz} = \frac{i}{2}\kappa A_4 + 2i\gamma A_1 A_2 A_3^* \qquad (2.5.4)$$

where $A_K$ is the scalar field amplitude. $\kappa = \Delta\beta + \gamma(P_1 + P_2)$ is called the phase-mismatch parameter. It incorporates phase mismatch originating from fiber dispersion as well as the imbalance in the nonlinear phase shift experienced by the two pumps, and the signal and idler. P1 and P2 are the pump powers. Equations (2.5.3) and (2.5.4) can be used to find equations for the evolution of signal and idler powers $P_3 = |A_3|^2$ and $P_4 = |A_4|^2$

$$\frac{dP_3}{dz} = \frac{dP_4}{dz} = 2\sqrt{P_1 P_2 P_3 P_4}\sin(\theta), \qquad (2.5.5)$$

where $\theta = \phi_3 + \phi_4 - \phi_1 - \phi_2$ describes the accumulated phase mismatch among the four waves Here $\phi_j$ is the phase of the field Bj, i.e., $A_j = \sqrt{P_j}e^{(i\phi_j)}$. When the two pumps are assumed to remain undeleted, $\phi_1$ and $\phi_2$ maintain their initial values and the accumulated phase mismatch is governed by

$$\frac{d\theta}{dz} = \kappa + 2\gamma\cos\theta\frac{\sqrt{P_1 P_2}(P_3 + P_4)}{\sqrt{P_3 P_4}}. \qquad (2.5.6)$$

Equation (2.5.3) shows clearly that the growth of the signal and idler waves inside a fiber is determined by the phase-matching condition. When $\theta = \frac{\pi}{2}$, the signal and idler extract

energy from the two pumps. In contrast, when $\theta = -\frac{\pi}{2}$, energy can flow back to the two pumps from the signal and idler. If only the two pumps and the signal are launched into FOPA initially, the idler wave is automatically generated by the FWM process. This can be seen from Eq. (2.5.4). Even if $A_4 = 0$ at z = 0, its derivative is not zero as long as $A_3(0)$ is finite. Integrating this equation over a short fiber section of length Δz, one obtains $\Delta A_4 \approx 2iA_1 A_2 A_3^*(0)\Delta z$. The factor of i provides an initial value of $\frac{\pi}{2}$ for θ and shows that the correct phase difference is automatically picked up by the FWM process. If k = 0 initially (perfect phase matching), Eq. (2.5.6) shows that θ will remain frozen at its initial value of. However, if k 6= 0, θ will change along the fiber as dictated by Eq. (2.5.6) and energy will flow back into the two pumps in a periodic fashion. Thus, phase matching is critical for signal amplification and idler generation.

## 2.6 Single-Pump Parametric Amplifiers

In this Section the focus is on a simpler case in which a single intense pump is launched into a fiber together with the signal, and a single idler wave is generated through the degenerate FWM process. FWM equations in the case of single-pump FOPAs can be derived starting from Eqs. (2.4.12) and (2.4.13). Assuming for the sake of simplicity that all fields are linearly polarized along x-axis, $|A_k\rangle = A_k \hat{x}$ , simple scalar FWM equations can be obtained by putting $A_2$ =0 in Eq. (2.4.12) and replacing both $A_1$ and $A_2$ by $\frac{A_1}{\sqrt{2}}$ in Eq. (2.4.13). With these simplifications, signal and idler equations become:

$$\frac{dA_3}{dz} = \frac{i}{2}\kappa A_3 + i\gamma A_1^2 A_4^* \qquad (2.6.1)$$

$$\frac{dA_4}{dz} = \frac{i}{2}\kappa A_4 + i\gamma A_1^2 A_3^* \qquad (2.6.2)$$

where in this case $k = \Delta\beta + 2\gamma P_1$ . Equations (2.6.1) and (2.6.2) can easily be solved to find the signal gain. These equations can also be integrated in an elegant fashion by making use of the Pauli spin matrices. With the use of Pauli spin matrices Eqs. (2.6.1) and (2.6.2) can be written as

$$\frac{d}{dz}\begin{bmatrix} A_3 \\ A_4^* \end{bmatrix} = \vec{g}.\vec{\sigma}\begin{bmatrix} A_3 \\ A_4^* \end{bmatrix} \qquad (2.6.3)$$

where $[A_3, A_4^*]^T$ does not correspond to any physical vector but is merely a mathematical construct and $g = [\frac{iK}{2}, -\gamma \,\mathrm{Im}(A_1^2), -\gamma \,\mathrm{Re}(A_1^2)]$ is a constant vector. Equation (2.6.3) can be integrated formally to obtain

$$\begin{bmatrix} A_3(L) \\ A_4^*(L) \end{bmatrix} = \exp(\vec{g}.\vec{\sigma}L) \begin{bmatrix} A_3(0) \\ A_4^*(0) \end{bmatrix} \qquad (2.6.4)$$

The exponential matrix can be expanded as follows

$$\exp(\vec{a}\cdot\vec{\sigma}) = \cosh a + \hat{a}\cdot\vec{\sigma}\sinh a, \qquad (2.6.5)$$

Where $a$ is any three-component vector with $a = \sqrt{a.a}$ and $a = \frac{a}{a}$ . Using this relation in Eq. (2.6.4), solutions for the signal and idler fields is found to be

$$A_3(L) = A_3(0)\left[\cosh(gL) + \frac{i\kappa}{2g}\sinh(gL)\right] + A_4^*(0)\frac{i\gamma A_1^2}{g}\sinh(gL), \qquad (2.6.6)$$

$$A_4(L) = A_4(0)\left[\cosh(gL) + \frac{i\kappa}{2g}\sinh(gL)\right] + A_3^*(0)\frac{i\gamma A_1^2}{g}\sinh(gL), \qquad (2.6.7)$$

where the parametric gain coefficient g is given by (with $P_1 = |A_1|^2$)

$$g = \sqrt{\vec{g}\cdot\vec{g}} = \sqrt{(\gamma P_1)^2 - (\kappa/2)^2}. \qquad (2.6.8)$$

Signal gain at the end of the fiber, defined as $G(\omega_3) = |A_3(L)/A_3(0)|^2$, can be found from Eq. (2.6.6). In particular, when there is no idler field at the input of the fiber, the signal gain becomes

$$G(\omega_3) = \left[1 + (1 + \kappa^2/4g^2)\sinh^2(gL)\right]. \qquad (2.6.9)$$

Equation (2.6.8) shows that the parametric gain is reduced by phase mismatch k and is maximum when k = 0. Both the nonlinear (SPM and XPM) and the linear effects (fiber dispersion) contribute to k. Although the nonlinear contribution is constant at a given pump power, the linear phase mismatch depends on the wavelengths of the three waves. To realize net amplification of the signal, the parametric gain g should be real. Thus, tolerable values of the linear phase mismatch $\Delta\beta$ are limited to the range $-4\gamma P_1 \le \Delta\beta \le 0$. The FOPA gain is maximum when the phase mismatches k approaches zero, or when $\Delta\beta = -2\gamma P_1$. This relation indicates that optimal operation of FOPAs requires some amount of negative linear mismatch to compensate for the nonlinear phase mismatch.

## **2.7** Basic Theory of Stimulated Raman Scattering [36]

On a molecular scale, the Raman nonlinearity arises from the *change in polarizability of a given molecule* that results from a displacement of some of its constituent atoms from the equilibrium position. The displacements usually involve two or more atoms that move in a symmetric manner, leading to no change in the overall dipole moment. Oscillation modes of this type are term Raman-active, as compared to dipole-active, modes; in the latter case, a dipole moment is induced through molecular or electronic displacement. With a Raman-active mode excited, additional light input may simultaneously excite a dipole-ative mode in the same molecule. However, the restoring forces associated with dipole-active mode (determining the polarizability) depend on the instantaneous locations of the component atoms. These, along with the polarizability, change as a result of the Raman-active mode displacements.

For an ensemble of identical molecules, the macroscopic polarization is written as

$$P(z,t) = \varepsilon_0 \chi E(z,t) = \varepsilon_0 N \alpha_P E(z,t) \tag{2.7.1}$$

Where N is the number density of molecules and $\alpha_P$ is the molecular polarizability(the polarizability associated with a single molecule). The nonlinear part of the polarization is obtained by expanding $\alpha_P$. The resulting time-varying polarizability can be described by the expansion

$$\alpha_p(z,t) = \alpha_{P0} + q(z,t)\left(\frac{\partial \alpha_p}{\partial q}\right)_{q=0} = \alpha_{p0} + \alpha_{P1} q(z,t) \tag{2.7.2}$$

Where $\alpha_{P1} = \left.\frac{\partial \alpha_P}{\partial q}\right|_{q=0}$ is the change in polarizability with displacement, evaluated at the equilibrium position. The displacement of a single atom $q(z,t)$ can be represented by the

function $q(z,t) = \frac{1}{2}Q(z)\exp(jw_{or}t) + c.c$ is the resonant (Raman) frequency and z is the propagation direction for both optical fields. When equation (2.7.2) is substituted into equation (2.7.1), it is found that the time varying displacement gives rise to nonlinear polarization terms that are up- and downshifted in frequency from that of the input light by an amount equal to the Raman frequency. Nonlinear part of the polarization expressed in (2.7.1), using (2.7.2) is

$$P_{NL}(z,t) = \varepsilon_0 N\alpha_{P1} q(z,t)E(z,t) \qquad (2.7.3)$$

Where $E(z,t) = E_s + E_p$ is the total field expressed as the sum of the Stokes and pump fields, respectively. These fields are assumed to copropagate in the medium and to have same polarization. They are given by

$$E_j(z,t) = \frac{1}{2}E_j \exp(i\omega_j t) + c.c \qquad (2.7.4)$$

where j is Stokes and pump frequency and the pump frequency is greater than the Stokes frequency. The displacement $q(z,t)$ is expected to be proportional to the difference frequency term in the product of $E_s$ and $E_P$. The actual form of $q(z,t)$ can be determined by solving an equation of motion for atom involved

$$m\frac{\partial^2 q}{\partial t^2} + m\xi_r \frac{\partial q}{\partial t} + k_s q = -eE(z,t) \qquad (2.7.5)$$

Where m is the mass of the atom, $\xi_r$ is damping coefficient and $k_s$ is the restoring force on the atom that give rise to resonant frequency. The solution of the equation (2.7.5) can be expressed as:

$$q(z,t) = \frac{\varepsilon_0\alpha_{p1}}{4m}\frac{E_P E_s^{*}\exp\left[-i(k_p - k_s)z\right]\exp[i(\omega_p - \omega_s)t]}{\omega_{0r}^2 - (\omega_p - \omega_s)_2 + i\xi_r(\omega_p - \omega_s)} + c.c \qquad (2.7.6)$$

The nonlinear polarizations (Stokes and Pump) are now constructed by substituting equation (2.7.6) into ( 2.7.3) and the result are:

$$P_{NL}^{\omega s}(z,t)=\frac{\varepsilon_0^2\alpha_{P1}^2}{8m}\left[\frac{E_P^2E_s\exp(-ik_sz)\exp(i\omega_st)}{\omega_r^2-(\omega_P-\omega_s)^2-i\xi_r(\omega_p-\omega_s)}\right]+c.c \qquad (2.7.7)$$

$$P_{NL}^{\omega P}(z,t)=\frac{\varepsilon_0^2\alpha_{P1}^2}{8m}\left[\frac{E_s^2E_P\exp(-ik_pz)\exp(i\omega_st)}{\omega_r^2-(\omega_P-\omega_s)^2-i\xi_r(\omega_p-\omega_s)}\right]+c.c \qquad (2.7.8)$$

Both polarizations must be included in wave equation to account for growth and depletion of the pump and Stokes fields. Equations (2.7.7) and (2.7.8) can be written in the form

$$P_{NL}^{\omega_i}(z,t)=\frac{1}{2}P_{NL}^{\omega_i}\exp(i\omega_it)+c.c \qquad (2.7.9)$$

Where i=s and p, and where the polarization phasors are

$$P_{NL}^{\omega_s}=\varepsilon_0\chi_r^{\omega s}E_P^2E_s\exp(-ik_sz) \qquad (2.7.10)$$

$$P_{NL}^{\omega_s}=\varepsilon_0\chi_r^{\omega s}E_P^2E_s\exp(-ik_sz) \qquad (2.7.11)$$

Using these with (2.7.7) and ( 2.7.8), we identify Raman susceptibilities. That for the Stokes wave is

$$\chi_r^{\omega_s}=\frac{\varepsilon_0N\alpha_{ps}^2}{4m}\left[\frac{\left[\omega_r^2-(\omega_P-\omega_s)^2\right]+i\xi_r(\omega_P-\omega_s)}{\left[\omega_r^2-(\omega_p-\omega_s)^2\right]^2+\xi_r^2(\omega_p-\omega_s)^2}\right]\approx-\frac{\varepsilon_0N\alpha_{p1}^2}{4m\omega_r\xi_r}\left(\frac{i+\delta_r}{1+\delta_r^2}\right) \qquad (2.7.12)$$

Where the normalized detuning parameter is $\delta_r\equiv\frac{2}{\xi_r}\left[(\omega_P-\omega_s)-\omega_r\right]$. The susceptibility associated with the pump wave is found to be the complex conjugate of (2.7.12):

$$\chi_r^{\omega_P} = \chi_r^{\omega s*} \approx -\frac{\varepsilon_0 N \alpha_{P1}^2}{4m\omega_r \xi_r}\left(\frac{i+\delta_r}{1+\delta_r^2}\right) \tag{2.7.13}$$

The fields and polarizations are now substituted into the wave equation (2.1.9), where $P_{NL} = P_{NL}^{\omega s} + P_{NL}^{\omega P}$ and $E = E_s + E_P$. We separate the wave equation into two coupling equations that describe the evolution with distance of the Stoke and pump field amplitudes:

$$\frac{dE_s}{dz} = -\frac{i\omega_s}{2nc}\chi_r E_P^2 E_s \tag{2.7.14}$$

$$\frac{dE_p}{dz} = -\frac{i\omega_p}{2nc}\chi_r E_s^2 E_p \tag{2.7.15}$$

Where n is refractive index and $\chi_r = \chi_r^{\omega s}$. The coupled equation can be rewritten in terms of wave intensities by

$$E_s^* \frac{dE_s}{dz} + E_s \frac{dE_s^*}{dz} = \frac{dE_s^2}{dz} = (-i\chi_r + i\chi_r^*)\frac{\omega_s}{2nc} E_s^2 E_p^2 \tag{2.7.16}$$

Finally, the wave intensity in W/m$^2$ is found for either frequency through $I = (n/2\eta)E_i^2$. Using this in (2.7.17) the results are as follow:

$$\frac{dI_s}{dz} = g_r I_s I_P - \alpha I_s \tag{2.7.17}$$

$$\frac{dI_P}{dz} = -\frac{\omega_p}{\omega_s} g_r I_s I_p \tag{2.7.18}$$

Where α attenuation coefficient and $g_r = \frac{\varepsilon_0 N \eta_0 \omega_s \alpha_{ps}^2}{2m\omega_r \xi_r c n^2}\left(\frac{1}{1+\delta_r^2}\right)$. Typically gr is determined through measurement.

# Chapter 3 Fiber Characterization

## 3.1 Non-linear Parameter

### 3.1.1 Introduction and motivation

Measuring the linear and nonlinear properties of devices and fibers is a crucial task in optical telecommunications since these properties directly impact the propagation of light sources. The requirements on the nonlinear properties vary significantly with the application. In transmission applications, the accumulated nonlinearity can become a source of impairment, but nonlinearity is mandatory when using solitons. Signal processing, pulse compression applications and amplification require a high nonlinear index or nonlinear parameter $\gamma$, since this decreases the required input peak power to achieve a given nonlinear phase shift and gain. The expression for the nonlinear parameter is

$$\gamma = \frac{n_2 \omega}{c A_{eff}} \qquad (3.1.1)$$

where $n_2$ is nonlinear- index coefficient, ω is the optical angular frequency, c is the velocity of light and $A_{eff}$ is the effective mode area.

The effective area, $A_{eff}$ of the highly nonlinear fiber is calculated by using the equation (3.1.2)

$$A_{eff} = \pi \left( \frac{MFD}{2} \right)^2 \qquad (3.1.2)$$

where MFD is the mode field diameter of the highly nonlinear fiber while the parameters such as c, ω and $n_2$ are obtained from [35]. We devise the following experiment to determine the Gaussian beam width at the far field and then we will calculate the MFD of the fiber by using the equation 3.1.3 (see Appendix C for complete derivation).

$$W_0 = \frac{w}{\left(1+\left(\frac{\pi w^2}{L\lambda}\right)^2\right)^{1/2}}$$
$$MFD = 2W_0 \qquad (3.1.3)$$

### 3.1.2 Experimental Setup to Determine the Mode Field Diameter

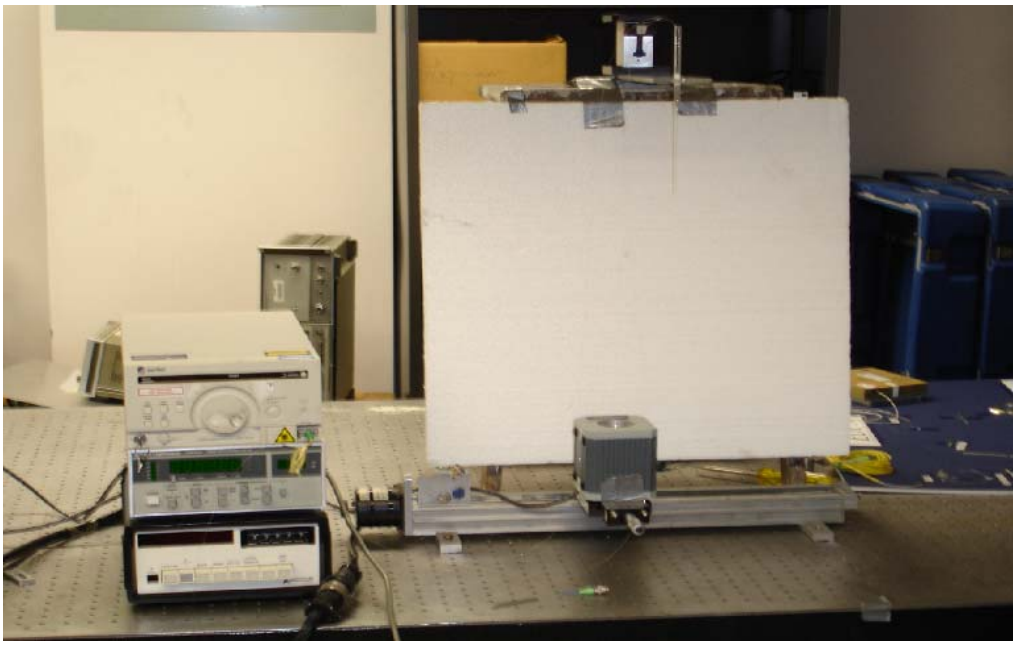

Fig. 3.1.1 Experimental setup

The experimental setup is presented in Figure 3.1.1 It consists of a tunable laser, the HNLF and a very sensitive power meter which is mounted on the XY stage. The position of the power meter at any given time can be precisely located since the stage is operated by a stepper motor controller. One end of the HNLF is connected to the laser while the other end is clamped to a holder. The fiber is placed at about 330mm away from the detector, as shown in Figure 3.1.1. The stepper motor controller scans the X axis of the stage until the detector measures the maximum power. Once the position is determined, we initialize the controller as the reference point. We then scan left and right of this reference position until the power level drops in each direction by 13.5% of its maximum.

## 3.1.3 Results

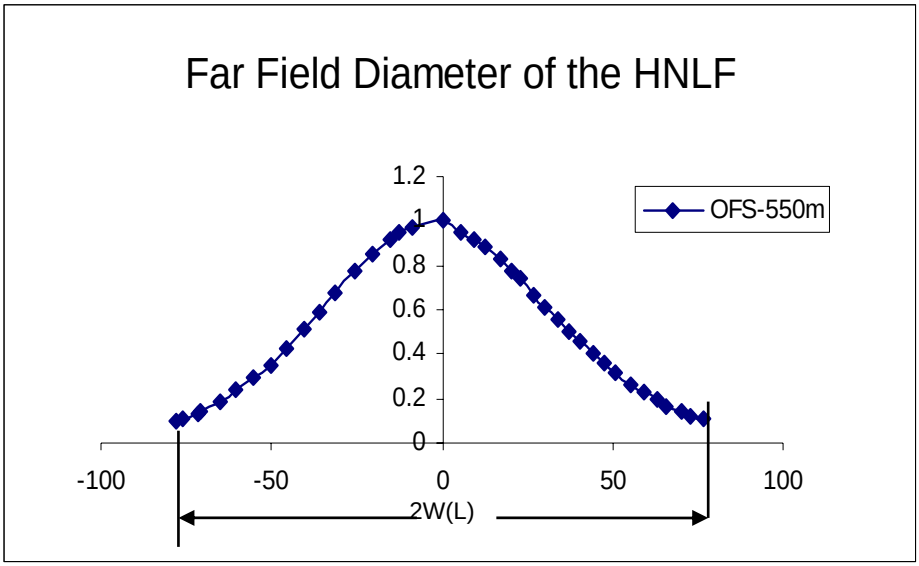


Fig. 3.1.2 Normalized beam intensity as a function of radial distance, ρ

The normalized beam intensity is plotted against the radial distance (X axis), ρ as Fig. 3.1.2 illustrates. It peaks when the radial distance, ρ=0 and drops monotonically by the factor $1/e^2$ or 13.5% at a radial distance W(z=330mm) as shown in Fig.5.2. Since 86% of the power is carried within the a circle of radius W(z), we regard W(z) as the beam radius and it is found to be 70.28 mm. Using our experimental parameters, z = L = 330mm and $\lambda$ =1550nm, the minimum waist $W_0$ is calculated to be 2.3μm (from Eq. 3.1.3). Finally, the nonlinear parameter, g is calculated to be $5.7 \times 10^{-3}$ $m^{-1}W^{-1}$(from Eq. 3.1.2)

## 3.2 Dispersion

### 3.2.1 Introduction

A medium exhibits chromatic dispersion if the phase constant $\beta$ for a wave within it varies nonlinearly with frequency. Signal distortion arising from group velocity dispersion occurs as the frequency components of signal propagate with different velocities. They thus emerge from the medium with a changed time relationship. In an optical waveguide, this effect arises from two mechanisms: 1) refractive index variations with the wavelength (change in n1 and n2 with $\lambda$) and 2) waveguide –related effects, an example of which is the change in the mode ray angle with wavelength. The interplay between these two mechanisms in optical fibers has led to a number of successful ways of minimizing net dispersion over a specified wavelength range by using special refractive index profile. Additional work has led to successful methods of compensating dispersion.

## 3.2.2 Group Delay and Dispersion parameter

Consider a small "spectral packet" of energy centered on frequency ω and having small spectral width. The group delay of the packet is given by the propagation distance z divided by the group velocity at frequency ω

$$\tau_g = z\frac{d\beta}{d\omega} = z\frac{d(nk_0)}{d\omega} = z\frac{d\lambda}{d\omega}\frac{d}{d\lambda}(nk_0) \tag{3.2.1}$$

where n is the refractive index and λ is the free-space wavelength, given by $\lambda = \frac{2\pi c}{\omega}$. At this stage, it becomes preferable to express parameters in terms of wavelength instead of frequency, as wavelength and wavelength spectra are usually measured experimentally. $\tau_g$ can be expressed in terms of wavelength through $\frac{d\lambda}{d\omega} = -\frac{2\pi c}{\omega^2}$ from which

$$\tau_g = -\frac{2\pi cz}{\omega^2}\left(\frac{k_0 dn}{d\lambda} + n\frac{dk_0}{d\lambda}\right) = \frac{z}{c}\left(n - \lambda\frac{dn}{d\lambda}\right) \tag{3.2.2}$$

$$v_g = \frac{z}{\tau_g} = \frac{c}{\left(n - \lambda\frac{dn}{d\lambda}\right)} = \frac{c}{N} \tag{3.2.3}$$

where the group index of the material is defined as

$$N \equiv n - \lambda\frac{dn}{d\lambda} \tag{3.2.4}$$

When considering wavelength measurements, it is useful to define the dispersion parameter $D(\lambda)$ which relates group delay changes to changes in wavelength:

$$D(\lambda) = \frac{dt_g}{d\lambda} \tag{3.2.5}$$

where $t_g = \frac{\tau_g}{z}$ is the group delay over a unit distance (1 km)

In order to find the dispersion parameter $D(\lambda)$ (see Equation 3.2.5), we will first determine the group delay and then we will differentiate it with respect to the wavelength.

### 3.2.3 Experimental Setup and Results

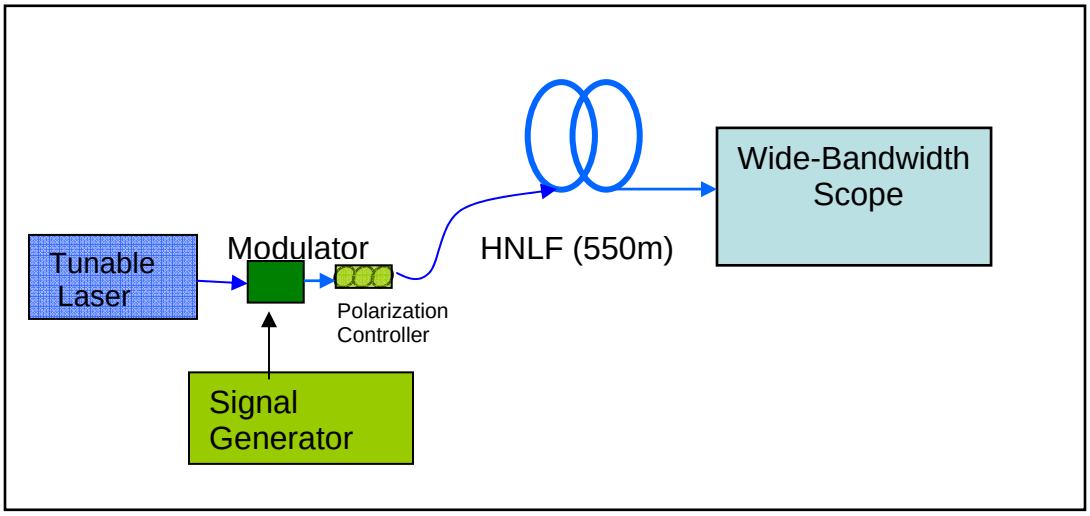


Fig.3.2.1. Experimental setup to measure the group delay.

The experimental setup in Fig. 3.2.1 consists of a tunable laser source, an amplitude modulator, a polarization controller, a HNLF and an Agilent broadband scope. The tunable laser source is first set at a certain wavelength and is then modulated to generate 100ps pulses. These pulses are channeled into the 550m long HNLF. A polarization controller is spliced in between the fiber and the modulator to maintain the state of polarization (SOP) of the pulses. The other end of the fiber is connected to the broadband scope, which is triggered electronically by the signal generator. The signal pulse and the triggering pulse are produced simultaneously which then travel in two different paths. The signal pulse travels though the fiber while the triggering pulse propagates through a short RF cable. The group delay is calculated by taking the time difference between the pulse that traveled through the fiber and the triggering pulse that propagated along the RF cable. We scan the tunable laser from 1510 nm to 1630 nm and measure the group delay

for every wavelength. The plot in Fig. 3.2.2 shows the profile of the group delay as a function of wavelength.

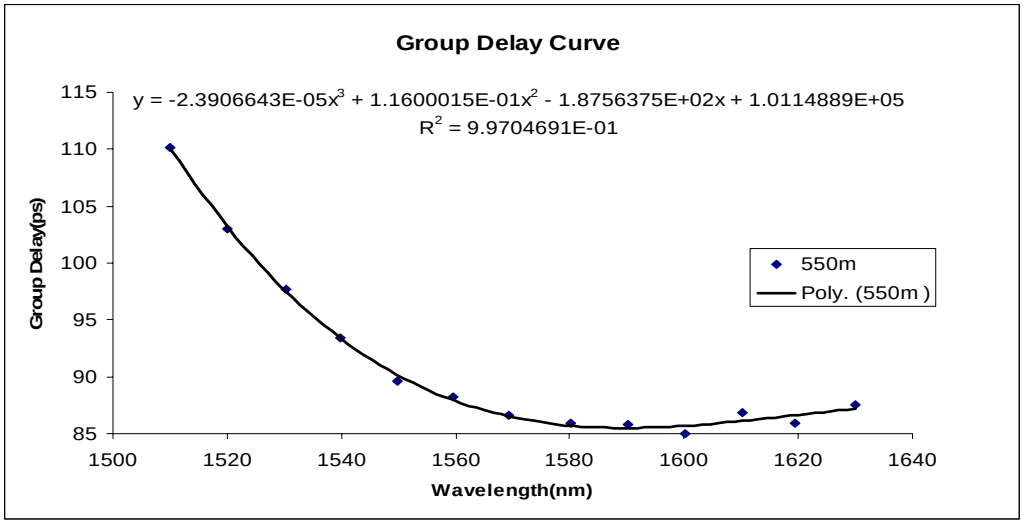


Fig. 3.2.2 A group delay as a function of the wavelength

The relationship between the group delay and the wavelength is then established by curve fitting the data. The dispersion coefficient, D( $\lambda$ ) is then calculated by taking the derivative of the third order polynomial (see Fig. 3.2.2). as shown in Fig. 3.2.3. The dispersion curve is negative below the zero dispersion wavelength (1590nm) while it becomes positive for any wavelength that is greater than the zero dispersion wavelength.

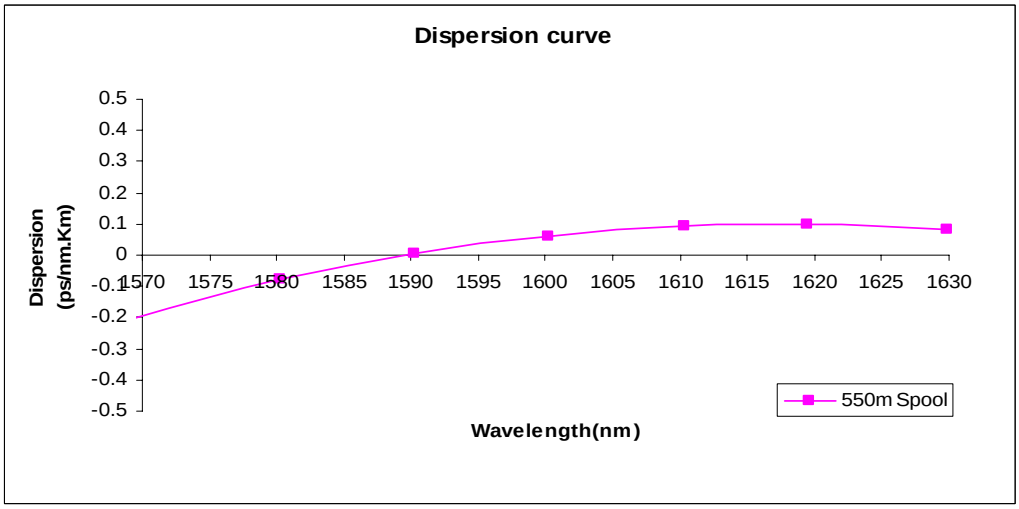


Fig. 3.2.3 Dispersion coefficient as a function of the wavelength of the HNLF

# Chapter 4

# Hybrid Raman/Parametric Amplifier (Unison Configuration)

## 4.1 Introduction and motivation

Two decades ago, the invention of erbium-doped fiber amplifiers (EDFAs) temporarily supplanted ongoing research on fiber Raman amplifiers (FRAs) and Optical parametric amplifiers (OPAs). However, due to the recent availability of high-power compact pump lasers, there has been renewed interest in FRAs and OPAs. We have exploited both of these nonlinear processes to develop a hybrid (FRA/OPA) wide bandwidth all-optical amplifier.

Raman amplifiers have attracted huge attention in recent years as the enabling technology for future long-haul, high-capacity optical communication systems. This is due to the fact that any wavelength within the transparency window of an optical fiber can be amplified by simply adjusting the pump wavelength [1]. This technology has been demonstrated to increase transmission capacity and span length in WDM transmission [2, 3]. In typical applications for transmission systems, FRAs showed superior performance, such as ultra-wide bandwidth, low noise, and suppressed nonlinearities. Discrete Raman amplifiers, using dispersion-compensating fiber (DCF) or

highly nonlinear fiber (HNLF), have also been shown to have good noise performance [4, 5] and better signal power budget.

On the other hand, optical parametric amplifiers utilize highly efficient four-wave mixing in an optical fiber, which requires phase matching between the optical signal and the optical pump [6]. One can obtain a bandwidth as large as 200 nm [7] and a gain as high as 49dB [8] by proper design of HNLF.

The increase in demand for larger bandwidth, lower noise figure and lower gain-ripple makes both RFAs and OPAs more attractive than traditional Erbium Doped Fiber Amplifiers (EDFAs) [9]. EDFAs are only limited to ~40nm bandwidth around 1545nm for a single amplifier, and to ~80nm bandwidth around 1565 nm for a multiple stage amplifier. Several studies indicate that, compared to the conventional EDFA, Raman-assisted EDFAs with a hybrid configuration yield lower noise figure (NF) and optical signal-to-noise ratio in long-haul transmission. For example, Seo *et al.* [10] demonstrated that a flat gain characteristic over the entire C and L bands could be achieved by using a Raman/EDFA hybrid amplifier, where C-band amplification was accomplished by direct transitions of Er ions, and L-band amplification was achieved by stimulated Raman scattering (SRS). Kurosawa *et al*. also demonstrated another type of single-pump hybrid amplifier (called Raman-assisted EDFA) to obtain both high pump efficiency and low noise performance [11]. However, with these hybrid configurations, bandwidth is still restricted by the Er ion states.

To enable RFAs to achieve ultra-wide bandwidth, many pumps at different wavelengths are necessary. However, many pump lasers work far below their maximum power to achieve a small gain variation and lower noise figure. Another problem

associated with the RFA design is the well-known quandary of pump interactions. The pumps interact with each other by drawing energy from one pump to another. Gain fluctuation and accompanied noise of individual amplifiers will be multiplied when the number of pumps increases [12].

RFAs and hybrid EDFA/RFA configurations have been widely used to achieve wide bandwidth amplification. However, the combined effect of Raman scattering and parametric amplification has received less attention. In optical fibers, E. Golovchenko *et al.* [13] have examined the phase mismatch parametric gain and have demonstrated that the gain depends strongly on the real part of the complex Raman susceptibility. More recently, Hsieh *et al.* [14] have examined the effect of the frequency detuning between the signal and the pump. Also, Joao *et al*. [15] characterized, both experimentally and theoretically, a Raman-enhanced parametric amplifier. Their focus was on gain enhancement effects, and on the coupling between the two nonlinear processes within a bandwidth where both processes showed strong amplification in a highly nonlinear fiber. They reported a 10dB gain enhancement in the S-band and a net 10dB conversion efficiency [15-18]. However, not much experimental work has been done to develop a wide-band hybrid amplifier by combining optical parametric amplification with Raman amplification.

In this thesis, we experimentally demonstrate an alternative way of combining RFA and OPA in a HNLF in order to extend the flat gain bandwidth of a Raman amplifier. This involves separating the Raman and parametric pumps by about 160 nm

and adjusting the relative pump powers in order to achieve a gain of over 15 dB and a gain ripple within 5 dB. It is expected that, by expanding the proposed hybrid RFA/OPA configuration, it will be possible to achieve ultra-wide bandwidth that is beyond the limits of RFAs alone or hybrid EDFA/ RFA amplifiers.

## 4.2 Experimental Technique

As a first approach, we will look at the possibility of enhancing the gain bandwidth of the amplifier with a configuration that we will call Unison. Next, we will compare it with that of a different configuration that we will call Tandem. The experimental test bed for the Unison configuration is shown in Fig. 4.2.1.

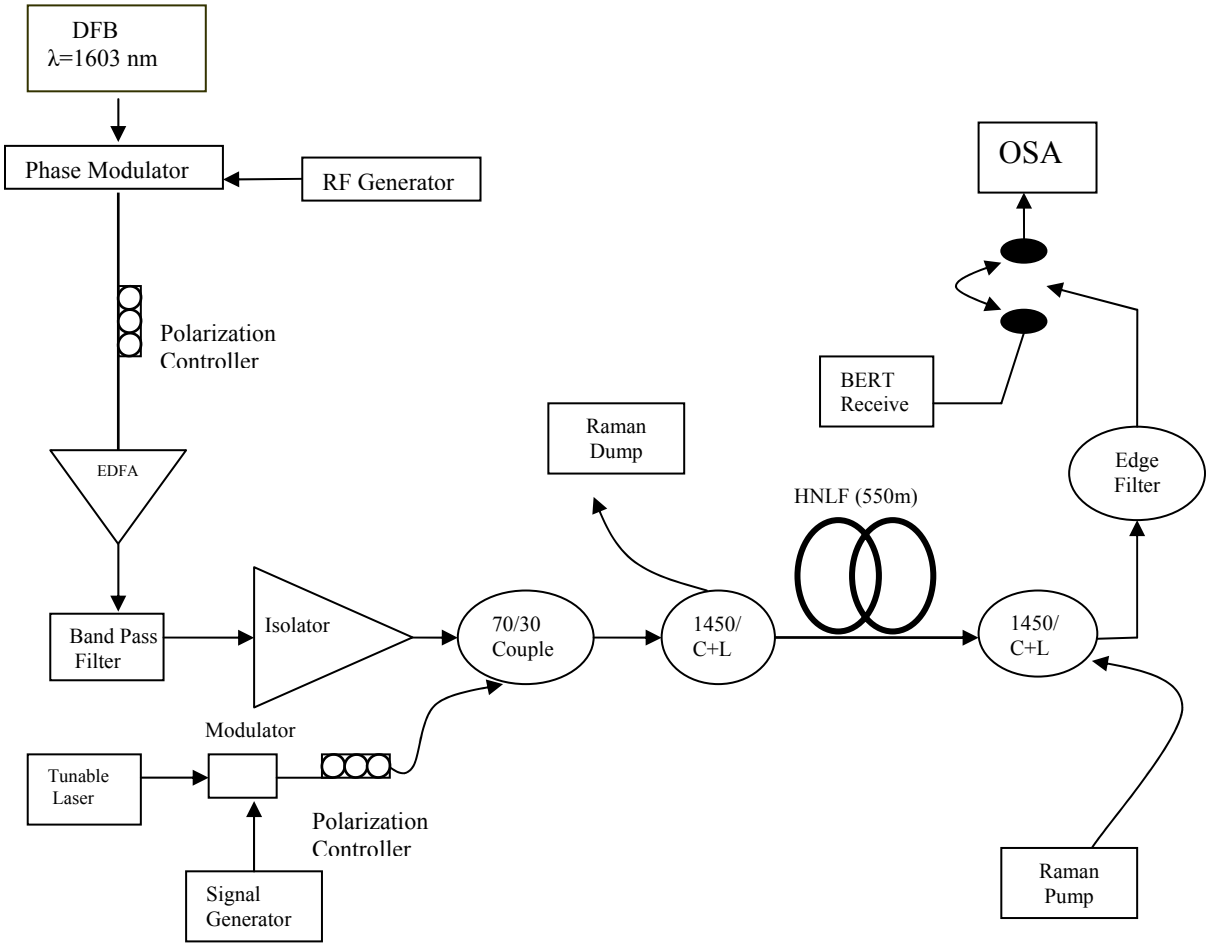


Fig.4.2.1. Experimental apparatus for investigating the Unison configuration of the Hybrid Raman/OPA fiber amplifier. BERT receiver: Bit error rate test -set receiver, DFB: distributed feed back laser, OSA: optical spectrum analyzer, WDM wavelength division multiplexer.

We used a DFB laser, centered at 1603nm, as a parametric pump source. It is then phase modulated by a combination of RF frequencies at 580 and 660 MHz to suppress stimulated Brillioun scattering (SBS) and to significantly enhance parametric gain. The laser beam at 1603nm was amplified using a high power EDFA. It was filtered with a 1 nm wide band pass filter and used as the parametric pump. A tunable laser (C+L band) is used as a signal source. If needed, the signal beam could be modulated using a Lithium Niobate Mach Zender amplitude modulator, driven by the amplified output of a pattern generator, producing a 10 Gb/sec NRZ pseudo random bit stream. The parametric pump and signal were then passed through a 1450nm/C+L band wavelength division multiplexer (WDM) before they were both launched into a 550m long HNLF fiber. A 1450nm/C+L coupler was spliced to the other end of the HNLF fiber to launch a counter propagating Raman pump (centered at 1450nm) into the HNLF. The amplified signal was analyzed after passing through an edge filter. The filter had about 1 dB insertion loss for wavelengths shorter than 1593nm and a blocking level of about 40dB for wavelengths longer than 1600nm. The signals were then analyzed in the wavelength domain, using an optical spectrum analyzer (OSA), and in time domain, using an Agilent 11982A O/E converter and sampling oscilloscope. Bit error rate analysis was performed using a bit error rate (BERT) analyzer.

## 4.3 Results

### 4.3.1 Gain Characterization

To investigate the interactions between the two pumps (Raman and parametric) and their effects on the gain, we first characterized the Raman and parametric amplification independently. On-off gain - the difference between the output signal power levels expressed in (dBm) with the pump turned on and the output signal turned off - was measured by scanning the tunable laser across the C+L band. Three sets of on-off gain curves, at three different power levels of the Raman pump, were measured (see Fig. 4.3.1.).

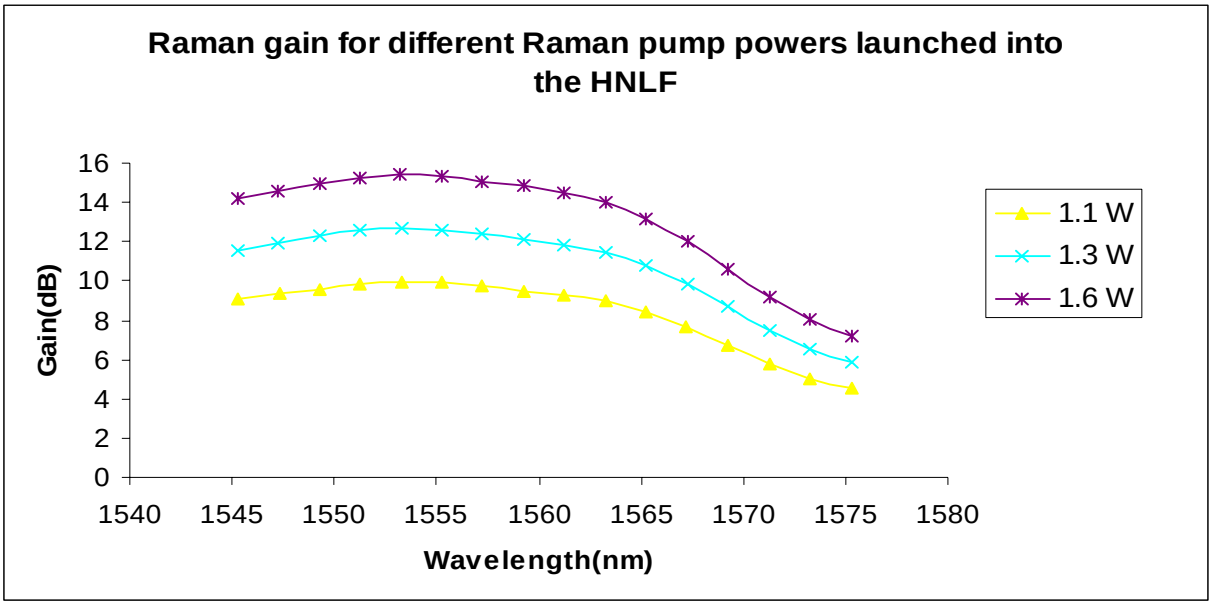


Fig.4.3.1. On-off gain curves for different Raman pump powers launched into the HNLF.

When the pump power was set at 1.6W, it was found that at 1555nm the on-off gain reached its maximum (15.2 dB) and gradually dropped as the signal wavelength tuned across the L band. Similarly, as shown in Fig.3.3.2, three gain curves were obtained by only turning on the parametric pump. It was observed that when the pump was set at

0.69W and the signal wavelength was tuned to 1584nm, the on-off gain reached its peak (14.5 dB).

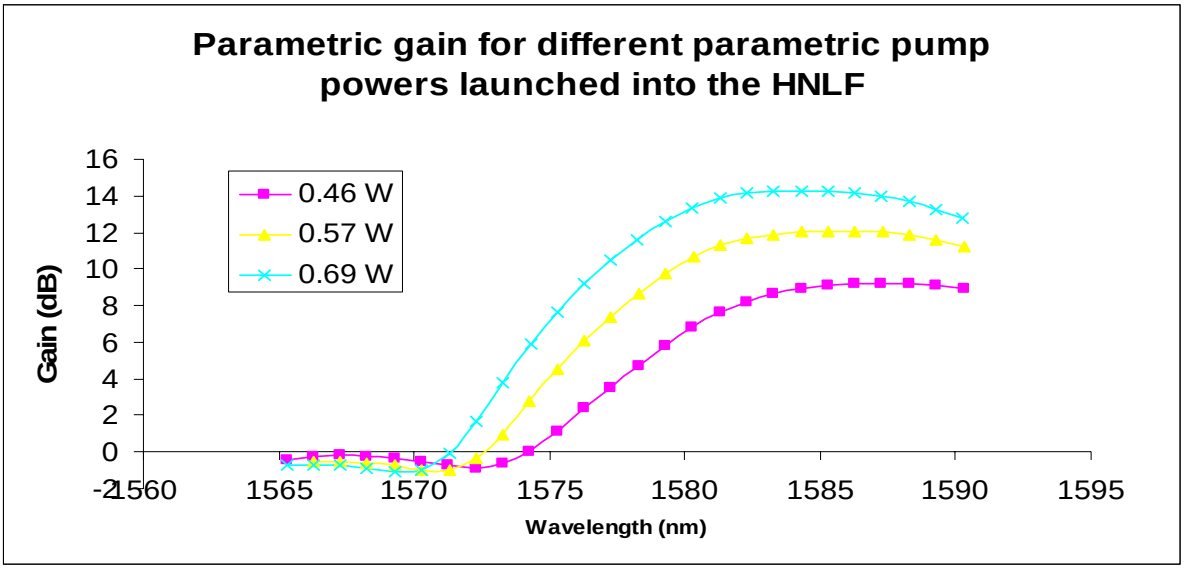


Fig.4.3.2 Parametric gain for different parametric pump powers launched into the HNLF fiber

We then repeated these measurements using the same pump powers, but with both pumps turned on (see Fig.4.3.3).

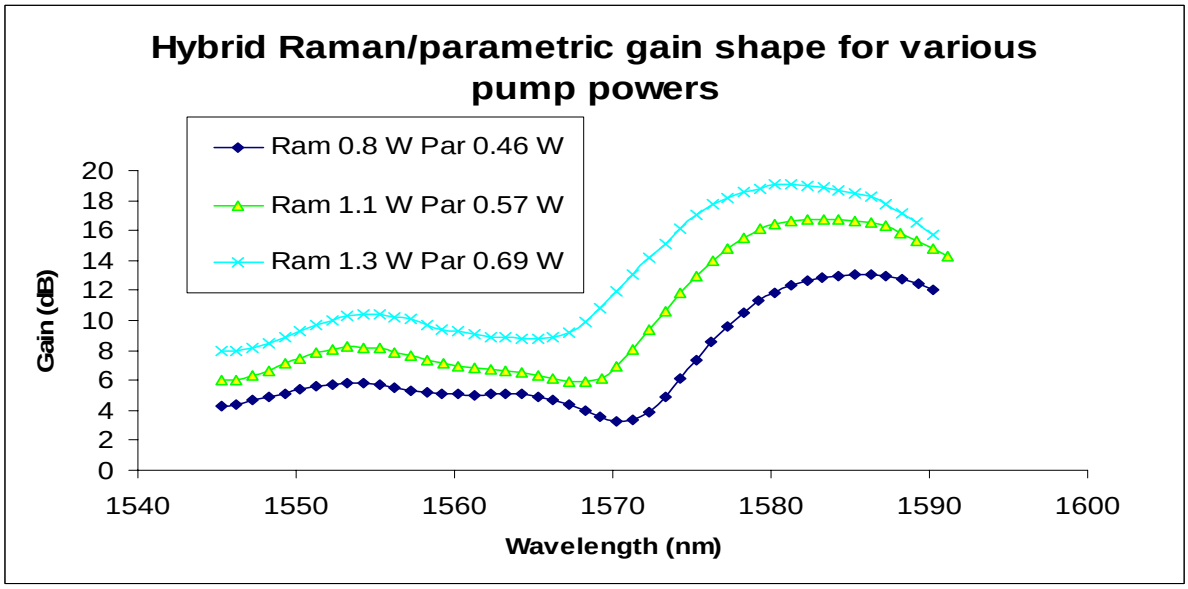


Fig.4.3.3. Hybrid Raman/ parametric gain shape for various pump powers.

Note the change in the on-off gain profile of the amplifier. The gain at 1555 nm was no longer 15 dB but dropped to about 10dB, while the gain at 1584nm was increased to 18dB.

This drop in the Raman gain region can be explained by monitoring the Raman dump port (See Fig.4.2.1). The Raman pump was set at 1.6W, while the parametric pump (fixed at 0.69W) was scanned from 1580nm to 1615nm and the power at the dump port was recorded. Next, we turned off the parametric pump and measured the power at the dump port with only the Raman pump turned on. Using these measurements, we calculated the power that was transferred from the Raman to the parametric pump, as shown in Fig. 4.3.4.

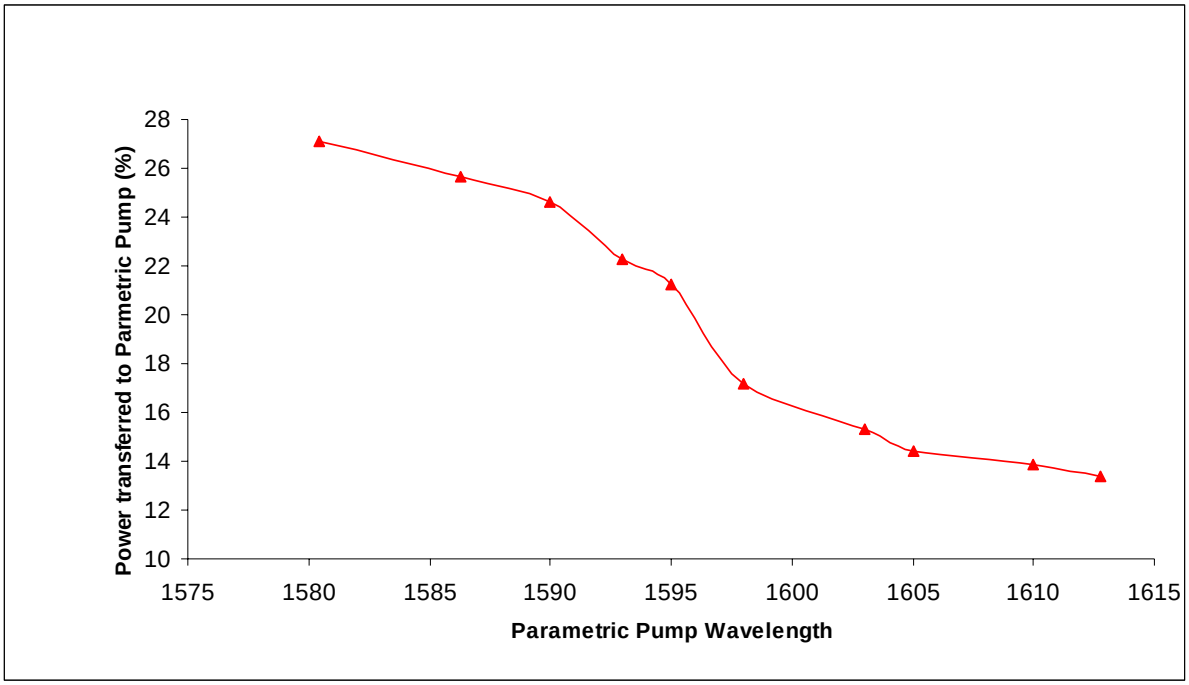


Fig.4.3.4. Plot of Power transferred to the parametric pump as a function of parametric pump wavelength.

The plot showed that the magnitude of the power that was transferred depended upon the proximity of the parametric pump wavelength to the Raman gain region. The amplified spontaneous emission (ASE) due to the Raman pump (λp=1450nm) was also monitored, as shown in Fig.4.3.5. It was found that it peaked at 1555nm and then gradually dropped beyond 1600nm. The power that was transferred from the Raman to the parametric pump followed the same trend as that of the ASE.

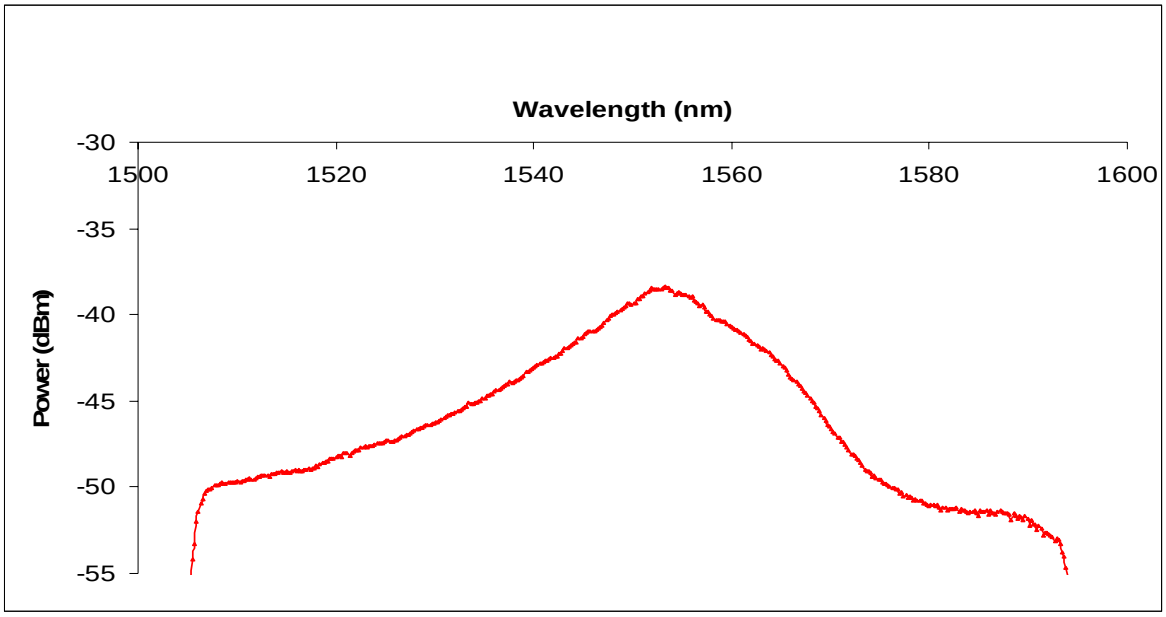


Fig.4.3.5. ASE gain profile for the Raman pump set at 1450nm

In Fig. 4.3.6, curves A and B show the ASE profiles when the Raman pump (λp=1450nm) power is set at 1.6W and the parametric pump (λp=1603nm) power is set at 0.412W respectively, while curve C represents the ASE when both pumps are launched simultaneously into the HNLF fiber. We also monitored the dump port and found that about 15% of the Raman pump power was transferred to the parametric pump, as

predicted by the curve in Fig. 4.3.4. To verify the power transfer, we turned off the Raman pump and increased the parametric pump by an additional 0.245W (15% of Raman Pump power) and then plotted the ASE produced by the parametric pump only (See fig. 4.3.6, curve D). Next, we reduced the Raman pump power by 15% to 1.36W and recorded the ASE.

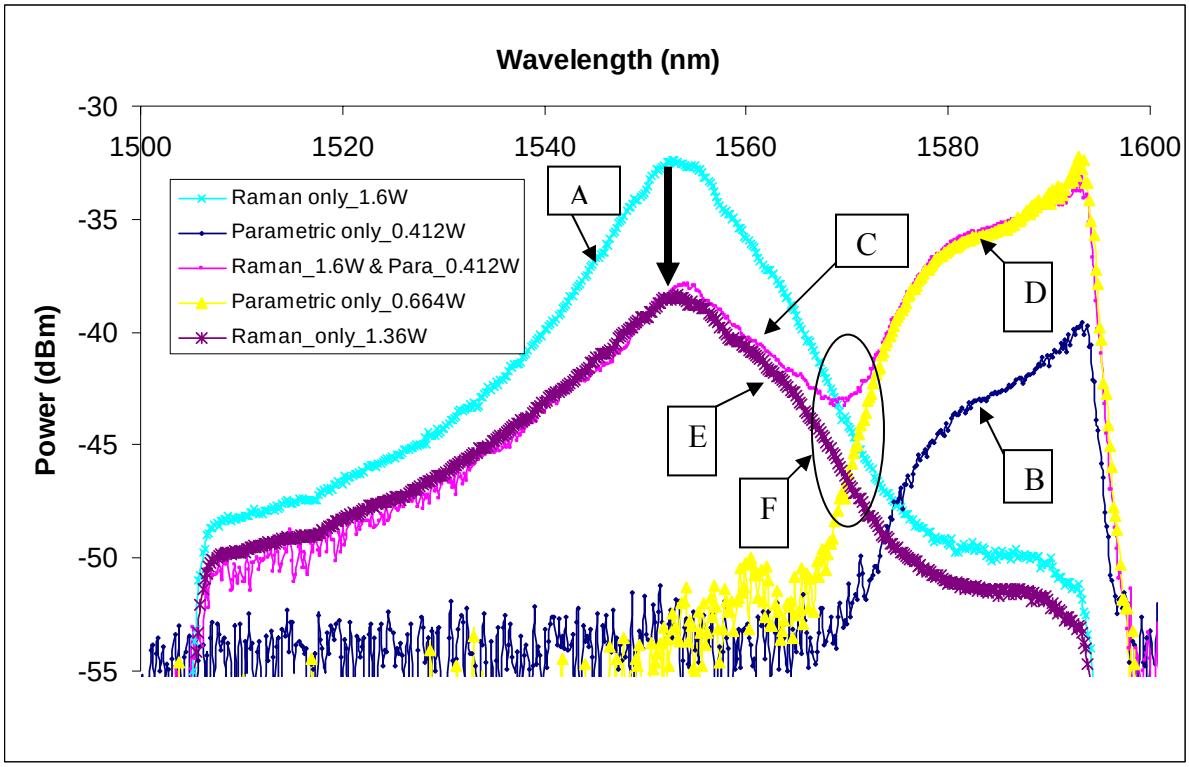


Fig.4.3.6. ASE curves: Curve A represents ASE due to Raman pump set at 1.6W. Curve B represents ASE due to parametric pump set at 0.412 W. Curve C represents ASE due to both Raman and parametric pumps set at 1.6W and 0.412W respectively. Curve D represents ASE due to parametric pump set at 0.664 W. Curve E represents ASE due to Raman pump set at 1.36W

The resulting ASE measurements are shown in Fig. 3.3.6 curve E. Figure 4.3.6 also shows that the parametric and Raman gain regions of curves D and E are in good agreement with curve C. This implies that in the Unison configuration the Raman pump loses its power to the parametric pump, thereby decreasing the Raman gain, while increasing the parametric gain (See Fig. 4.3.3).

Finally, we made the appropriate power adjustments to the pumps in order to minimize gain variation across the amplification bandwidth (Fig. 4.3.7). The gain measurements in the region of strong parametric gain were observed to depend on the relative polarization of the signal compared to the parametric pump polarization. However, once this relative polarization was set, the dependence as the wavelength was scanned was small.

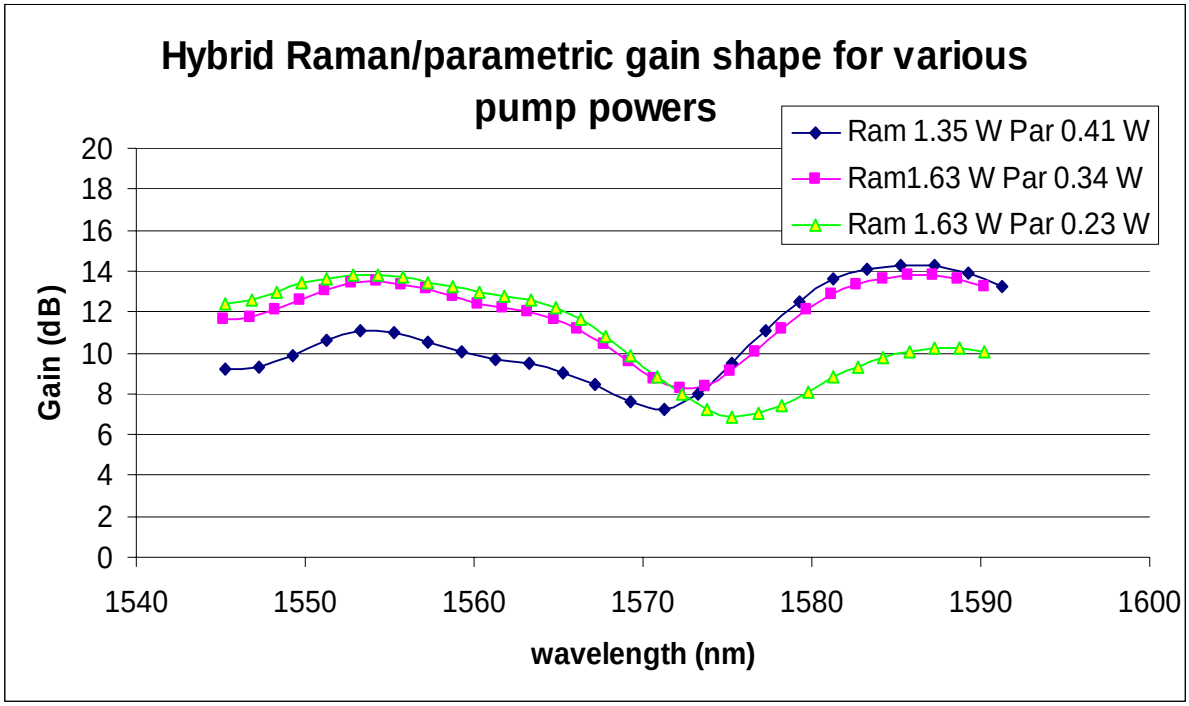


Fig.4.3.7. Unison configuration: Gain curves showing the optimization of the gain flatness

## 4.4 Time domain studies for Unison

Time domain studies for the Unison configuration were carried out by setting the Raman pump to 1.63W and the parametric pump to 0.34W. We measured the BER performance of the amplifier at various wavelengths. Eye diagrams and BER curves are presented for two signal wavelengths, corresponding to the two peaks in the gain spectrum. Figs. 4.4.1(a) and 4.4.1(b) show the eye diagrams when the signal wavelength is at 1554 nm and 1589 nm respectively.

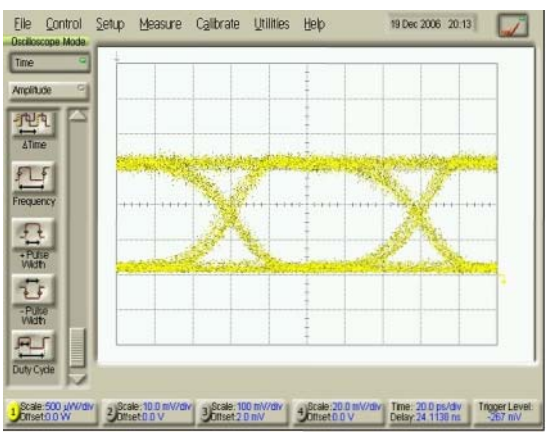


(a)

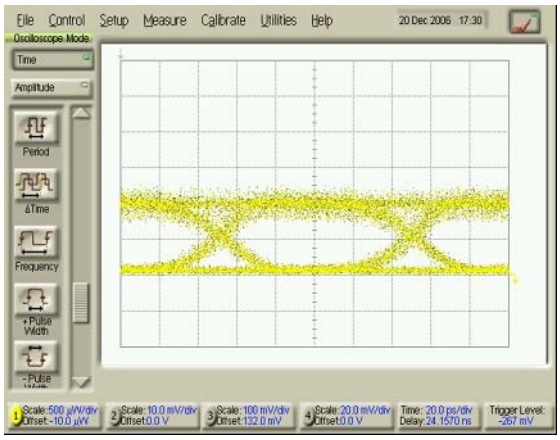


(b)

Fig.4.4.1. Unison configuration: (a) Eye diagram at the output of the amplifier when the signal wavelength is 1554 nm. (b) Eye diagram at the output of the amplifier when the signal wavelength is 1589 nm

The eye at 1589 nm shows some distortions on the top rail. The distortions seen in the top rail of Fig. 4.4.1 (b) are reflected on the bit error rate performance. Receiver performance was characterized as a function of received optical power. This is shown in Fig. 4.4.2, where a 3 dB power penalty is observed at the 1589 nm wavelength, whereas

no power penalty is observed at 1554 nm. The 3dB power penalty, close to the parametric gain region, is due to stochastic gain fluctuation and stimulated Brillouin scattering induced noise [16-17]. We performed a heterodyne detection experiment and found that heterodyne beats, arising from the output of the amplifier and the parametric pump, produce a frequency shift of 10~11 GHz. The SBS is pump power dependent and was much more significant at 0.63 W than at 0.34 W. Although in the Unison configuration the parametric pump is set at only 0.34W, the transfer of about 15% of the total Raman pump power (See Fig. 4.3.4) to the parametric pump increases SBS noise level and deteriorates the signal significantly.

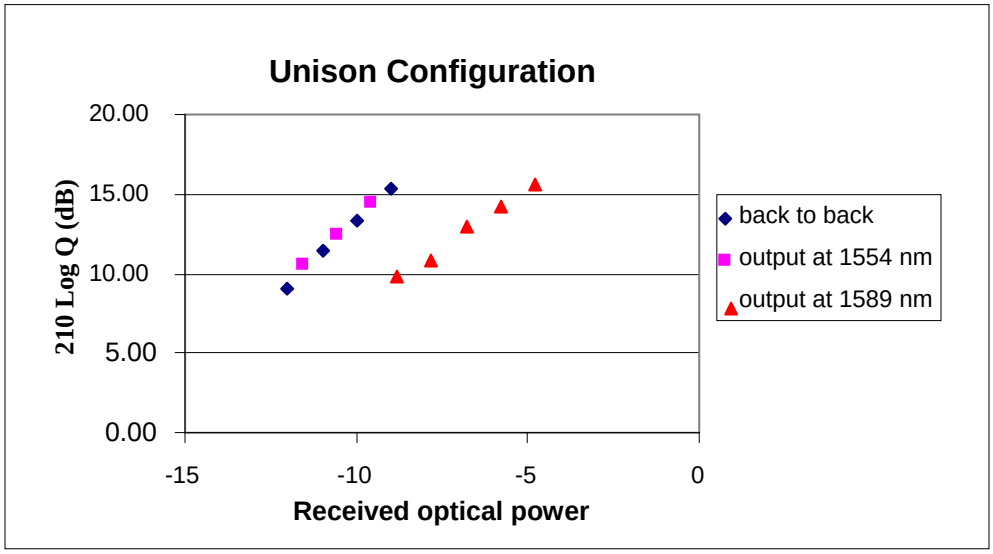


Fig.4.4.2. Unison configuration: A plot of the receiver performance as a function of received optical power shows a power penalty of about 3 dB for signals near the peak of the right hand gain peak but no power penalty for signals near the peak of the left hand gain peak.

# 4.4 Hybrid Raman/Parametric Amplifier (Tandem Configuration)

### 4.4.1 Experimental Technique

In the Tandem configuration, parametric and Raman amplification were carried out separately in two 550m HNLF fibers, as shown in Fig. 4..4.3. In this setup, the Raman and parametric pumps did not interact with each other, thereby preventing energy transfer from the Raman pump to the parametric pump.

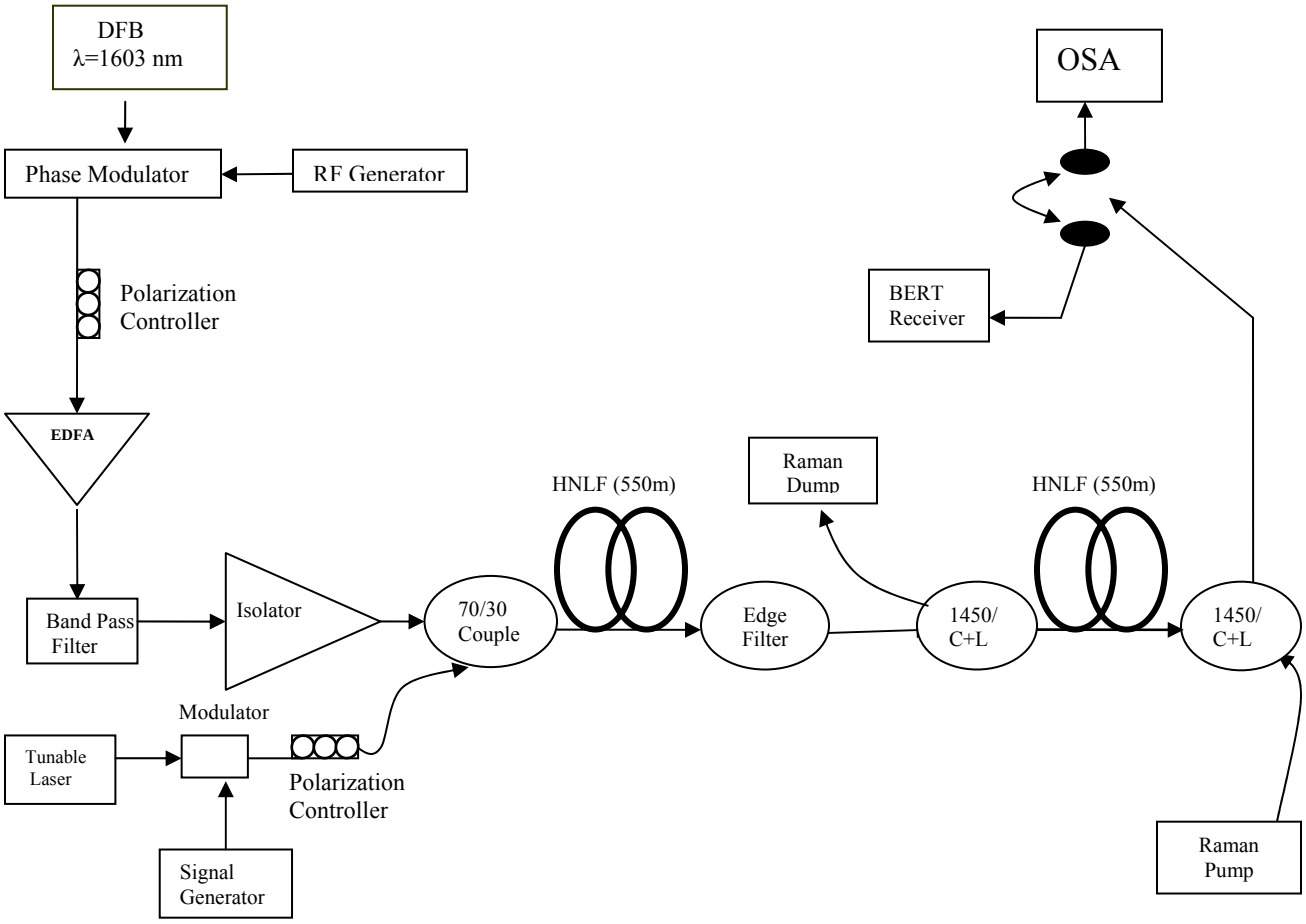


Fig.4.4.3. Experimental setup for investigating the Tandem configuration of the Hybrid Raman/OPA fiber amplifier. BERT receiver: Bit error rate test -set receiver, DFB: distributed feed back laser, OSA: optical spectrum analyzer, WDM wavelength division multiplexer.

The co-propagating parametric pump and the signal were coupled using a 70/30 broad band coupler and were then launched into the first segment of HNLF fiber for parametric amplification. The other end of the HNLF fiber was connected to an edge filter where, the parametric pump at 1602.2nm was rejected and the signal was allowed to pass to the second segment of HNLF. The two ends of the second segment were spliced to 1450nm/C+L band couplers. These were used to couple the Raman pump into the HNLF and then to dump the Raman pump, while allowing the signal to pass through. The resulting signal's spectral and temporal characteristics were then measured and bit error rate analysis was performed using the bit error rate test-set BERT analyzer.

## 4.5 Results

### 4.5.1 Gain Characterization

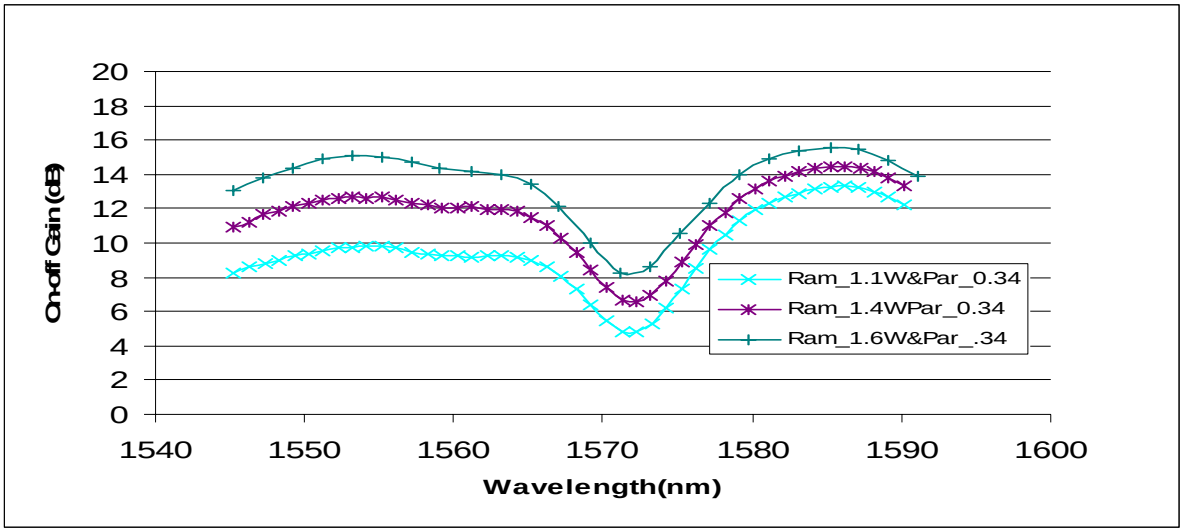


Fig.4.5.1. Tandem configuration: Gain curves showing the optimization of the gain flatness

In the Tandem configuration (See Fig. 4.4.1), the parametric pump wavelength ($\lambda p$=1602.2nm) is filtered out using an edge filter. Signals within the parametric gain region (wavelength longer than 1573nm), undergo amplifications while the signals outside the gain region experience fiber attenuation. The signal is then passed onto the second HNLF where it encounters Raman amplification. Fig. 4.3.5 shows the gain profile of the Raman pump. It peaks at 1555nm and gradually drops down in the L band region. This shows that wavelengths around 1570nm-1580nm (see Fig. 4.3.6, region E) are amplified by both the parametric pump and the Raman pump as the two gain regions overlap. In this configuration, we can minimize the gain variation by proper adjustment of the overlap of the gain regions. Higher gain levels in both regions were achieved and no additional power adjustments were required to flatten the gain as shown in Fig.4.5.1.

## 4.5.2 Time domain studies for Tandem

In the Tandem configuration, SBS remained low, since there was no transfer of power between the pumps. The power level of the parametric pump stayed at 0.34W and the generated SBS remained low at this level. The eye diagrams (when the signal is at 1554 nm and 1589 nm) are shown in Fig. 4.5.2 (a) and Fig. 4.5.2 (b) respectively

(a) (b)

Fig.4.5.2. Tandem configuration (a) Eye diagram at the output of the amplifier when the signal wavelength is 1554 nm. (b) Eye diagram at the output of the amplifier when the signal wavelength is 1589 nm

The eye at 1589 nm shows some distortions on the top rail and a power penalty of 1dB is observed. The receiver performance as a function of received optical power is shown in Fig. 4.5.2.

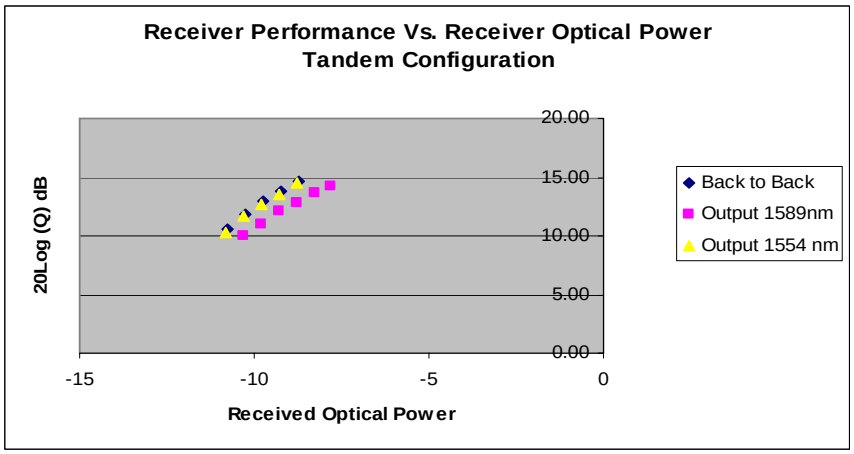


Fig.4.5.3. Tandem configuration: A plot of the receiver performance as a function of received optical power shows a power penalty of about 1 dB for signals near the peak of the right hand gain peak but no power penalty for signals near the peak of the left hand gain peak.

Many experiments have been performed which show that SBS in an optical fiber not only leads to saturation of the average power but also dramatically increases the relative noise of the signal [19-21]. Additionally, Nguyen *et al.* [22] presented a model of Brillouin scattering, which showed that the spontaneous scattering mechanism is responsible for generating noise for the stimulated process. Kylemark e*t al*. [23] have theoretically shown that the noise figure (NF) of parametric amplifiers depended mainly on the signal input power and the signal wavelength. The noise variance caused by the pump source is proportional to the square of the input signal power [23-24]. Thus, the noise becomes significant when the signal power is high.

The intensity fluctuations of the optical pump can come from mainly three different sources. The first source comes from spontaneously emitted photons generated during lasing. This process causes the output power to fluctuate and it is quantified by the relative intensity noise (RIN). The second source of intensity fluctuation is due to the use

of an EDFA to increase the power of the parametric pump. The EDFA adds ASE to the pump. The variance of the pump power due to ASE can be written as $\sigma^2_{P_p-ASE} = 4R^2 P_p S_{ASE} \Delta f$ , where $S_{ASE} = \eta_{sp}(G_{EDFA} - 1)h\nu$ , $\Delta f$ is the electrical bandwidth of the filter at the receiver, and R is the responsivity of the detector [23-24]. We were able to reduce the noise due to this process by using a very narrow bandwidth (1nm) optical filter. The third process is generated from the quantum noise around the pump which has a spectral density of $S_{QN} = \frac{h\nu}{2}$. The contribution from this process is usually small and can be neglected.

## 4.6 Conclusion

We have experimentally demonstrated that, by combining parametric and Raman processes in one unit, we are able to increase the gain bandwidth by extending the gain region to the longer wavelength side of the Raman gain. The flat gain can be achieved by two different configurations - Unison and Tandem. Gain of about 14-15 dB, with a gain flatness of 5-6dB, is observed in both configurations. It is observed that in the Raman gain region (1545nm-1570nm) there is a negligible power penalty for both Unison and Tandem setups, whereas nearly 3dB power penalty is observed in the parametric gain region (1575nm to 1590nm) for Unison and about 1dB power penalty for Tandem setup. Based on our results, we surmise that with a hybrid amplifier, consisting of a sequence of such units, one can extend the flat gain bandwidth of telecommunication systems beyond the limits that have been previously demonstrated.

## 4.7 Mathematical Model

### 4.7.1. Using a Raman pump and a parametric pump

In order to simulate the experimental results, a mathematical model was developed. We assumed that the ASE noise, Rayleigh scattering (RS) and pump depletion by the signals are neglected in the coupling equations. The mathematical model is divided into two parts. In part A, the interaction between the co-propagating parametric pump and the counter propagating Raman pump was determined while, in part B, an expression for a net signal gain was established. In the following, the two parts are described in details.

**A. Analytical computation of the pump powers evolution**

In this section, an expression of pump power evolution for co-propagating parametric and counter propagating Raman pump is derived considering the pumps propagate alone (no presence of signal) but interacting with each other. The experimental data (See Fig. 3.4.5) confirms that the interaction between the pumps is due to the Raman effect, and hence, it can be represented by the following coupling equations (derivation is given in detail in chapter 2.7 ), which ignore spontaneous Raman scattering, Rayleigh backscattering, higher-order Stokes waves and other nonlinear processes:

$$\frac{dP_P}{dz} = \frac{g_{\lambda R}}{A_{eff}} P_R P_P - \alpha_P P_P \qquad (4.7.1)$$

$$\frac{dP_R}{dz^*} = -\frac{\omega_R}{\omega_P A_{eff}} g_{\lambda R} P_p P_R - \alpha_R P_R \qquad (4.7.2)$$

where $A_{eff}$ is the effective mode area of $P_R$ and $P_P$ are the Raman and parametric pump powers, $\omega_R$ and $\omega_P$ are the Raman and parametric pump frequencies, $\alpha_R$ and $\alpha_P$ are the attenuation coefficients of the Raman pump and parametric pump, respectively. We will assume $z^* = L-z$ (where L is the fiber length and z is the propagation distance), since the Raman pump is counter propagating. The gain parameter $g_{\lambda R}$ is calculated from the ASE measurements. Note that Eqs. (4.7.1)-(4.7.2) assume a depolarized Raman pump.

Using the initial conditions, $P_P(L=0Km) = 0.57W$ and $P_R(L=0.5Km)=1.1W$ and assuming that the Raman pump depletes, the approximate solution of Eqs. (4.7.1)-(4.7.2) can be obtained by dividing the total length of the fiber into small sections, each with length $\delta z$, and within each segment the light power can be considered to be constant. After iteration using the fourth order Runge-Kutta method, we can get the output power of the Raman and parametric pumps in each individual segment.

**B. Analytical computation of net gain**

Since the power of Raman and parametric pumps is known in every small segment $\delta z$, we calculate the signal gain due to the Raman pump, $g_R(\lambda, \delta z)$ and

parametric pump, $g_p(\lambda,\delta z)$ for any segment. Hence the net gain for the entire length (L) of the fiber due to Raman pump only, $g_R(\lambda,L)$ and the net gain due to parametric pump only $g_p(\lambda,L)$ can be expressed as follows:

$$g_R(\lambda,L)=(g_R(\lambda,\delta z_1)g_R(\lambda,\delta z_2).....g_R(\lambda,\delta z_n)) \quad (4.7.3)$$

$$g_P(\lambda,L)=(g_P(\lambda,\delta z_1)g_P(\lambda,\delta z_2).....g_P(\lambda,\delta z_n)) \quad (4.7.4)$$

where $g_R(\lambda,\delta z)$ and $g_P(\lambda,\delta z)$ are Raman and parametric gain in each segment

**a) Calculation of Raman gain for each segment,** $g_R(\lambda,\delta z)$

In order to calculate the Raman gain of individual segment $g_R(\lambda,\delta z)$, we will approach by using a small-signal model and will assume the Raman pump to be constant within that segment. In the small-signal regime where pump depletion due to signal λ, is neglected, the evolution of the signal and the pump power level may be derived from Eqs. (4.7.1)-(4.7.2). and can be written as follows:

$$\frac{dP_s}{dz}=\frac{g_{\lambda R}}{A_{eff}}P_R P_s-\alpha_s P_s \quad (4.7.5)$$

$$\frac{dP_R}{dz^*}=-\alpha_R P_R \quad (4.7.6)$$

where $P_s$ is the signal power. Note the first term of the Eq(4.7.2) is dropped in Eq(4.7.6) due to the assumption of non-depleted Raman pump. The solution for the small signal gain within the length, $\delta z$ can be derived by solving the coupling equations Eq(4.7.5) and Eq(4.7.6) analytically and can be expressed as follows:

$$g_R(\lambda, \delta z) = EXP\left( g_R \frac{P_R(\delta z)}{A_{eff}\,\alpha_R}\left(e^{\alpha_R \delta z} - 1\right) - \alpha_s \delta z \right) \tag{4.7.7}$$

where $P_{R(\delta z)}$ Raman pump power within the small segment , $\delta z$ .

**b) Calculation of parametric gain within the segment, $\delta z$**

Similarly, we will find parametric amplification within the infinitely small fiber segment, $\delta z$ by considering strength of strong parametric pump ( $P_P(dz)$ ) be constant within the fiber segment, $\delta z$ and co-propagating with a signal $\lambda$, in the fiber with nonlinear coefficient γ (we assume that γ > 0, as in the case of silica fiber). Small signal theory reveals the existence of parametric gain, which amplifies the signal, as well as an

idler arising at $\omega_i = 2\omega_p + \omega_s$ Amplification can be studied by means of the signal power gain in the length $\delta z$ of the fiber, given by:

$$g_P(\lambda, \delta z) = 1 + \left[ \frac{\gamma P_p(\delta z)}{g} \sinh(g \delta z) \right]^2 \tag{4.7.8}$$

The parametric gain g is given by :

$$g^2 = -\Delta k_0 \left( \frac{\Delta k_0}{4} + \gamma P(\delta z) \right) \tag{4.7.9}$$

where $\Delta k_0$ is the linear phase mismatch, which is expressed as:

$$\Delta k_0 = -\frac{2\pi c}{\lambda_0^2} \frac{dD}{d\lambda} (\lambda_p - \lambda_0)(\lambda_p - \lambda_s)^2 \tag{4.7.10}$$

where $\lambda_p$ and $\lambda_s$ are the pump and signal wavelengths, respectively, $\lambda_0$ is the fiber's zero-dispersion wavelength, D is the chromatic dispersion.

Therefore, the total signal gain, $G_T(\lambda, L)$ (dB) due the Raman and parametric pump for the entire length, L is calculated by summing Eqs (4.7.3) and (4.7.4) and can be expressed as:

$$G_T(\lambda, L) = 10\log(g_R(\lambda, L)) + 10\log(g_P(\lambda, L) \qquad (4.7.11)$$

And finally, the on/off gain is calculated by subtracting the total component losses ($L_T$ ) from the overall signal gain expressed by Eq. (4.7.11)

$$G_{(on/iff)} = G_T(\lambda, L) - L_T \qquad (4.7.12)$$

A computer model is developed by using the method described above. In Fig. 4.7.1 the triangles are experimental data and the circles represent the simulation data.

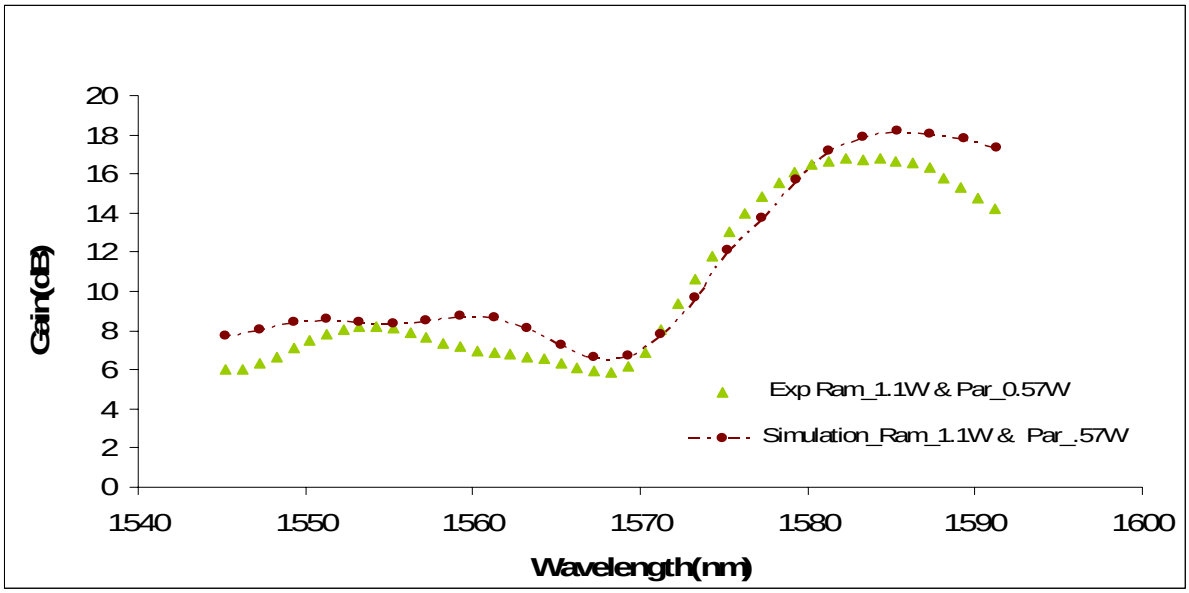


Fig.4.7.1 Gain profile of the Unison amplifier when both the pumps were turned on.

The simulated graph was in good agreement with the experimental data with the maximum relative error of 12% in the Raman gain region while 10% in the parametric gain region. Fig. 4.7.2 is a plot showing a gain flatness of 3dB that can be achieved by adjusting the pump powers.

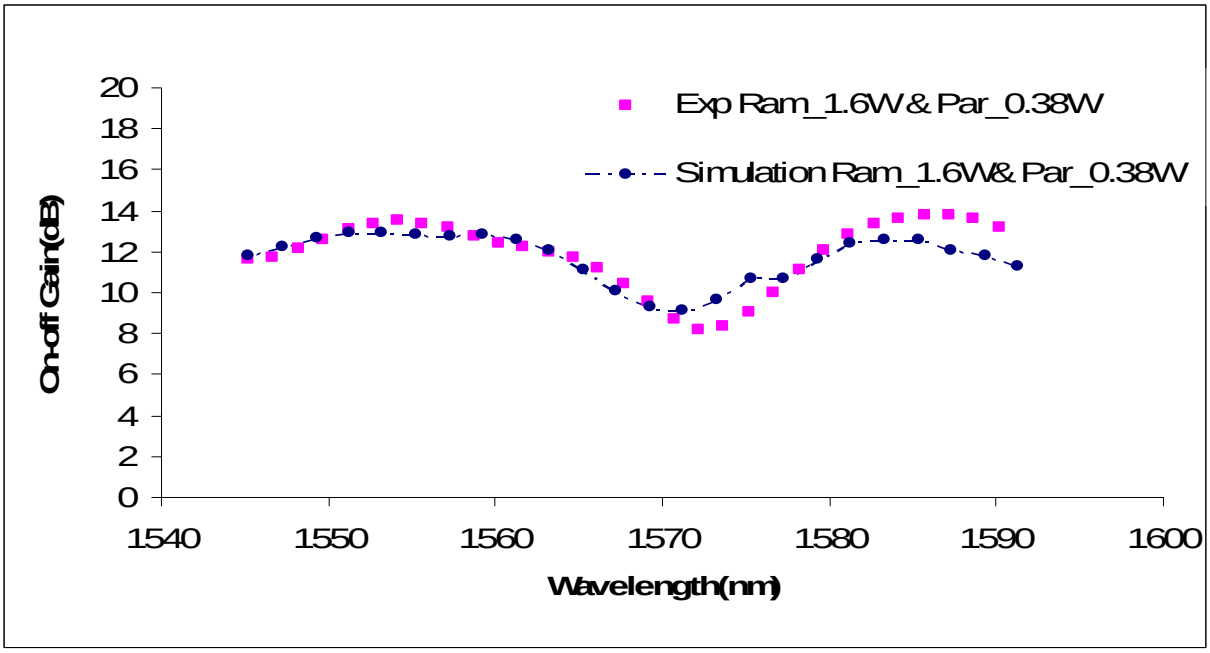


Fig.4.7.2. Unison configuration: Gain curves showing the optimization of the gain flatness

Using the same pump powers, a simulated graph (curve with diamonds) was plotted. The simulated curve and the experimental data were in good agreement with a maximum model/experiment difference of $\approx 2dB$ in the parametric region. The gain flatness differed by 1dB between the two curves. In the case of Tandem configuration, the model

predicted that the gain flatness could be minimized to about $\approx 4dB$ by tuning the Raman pump wavelength to 1453nm (See Fig. 4.7.3).

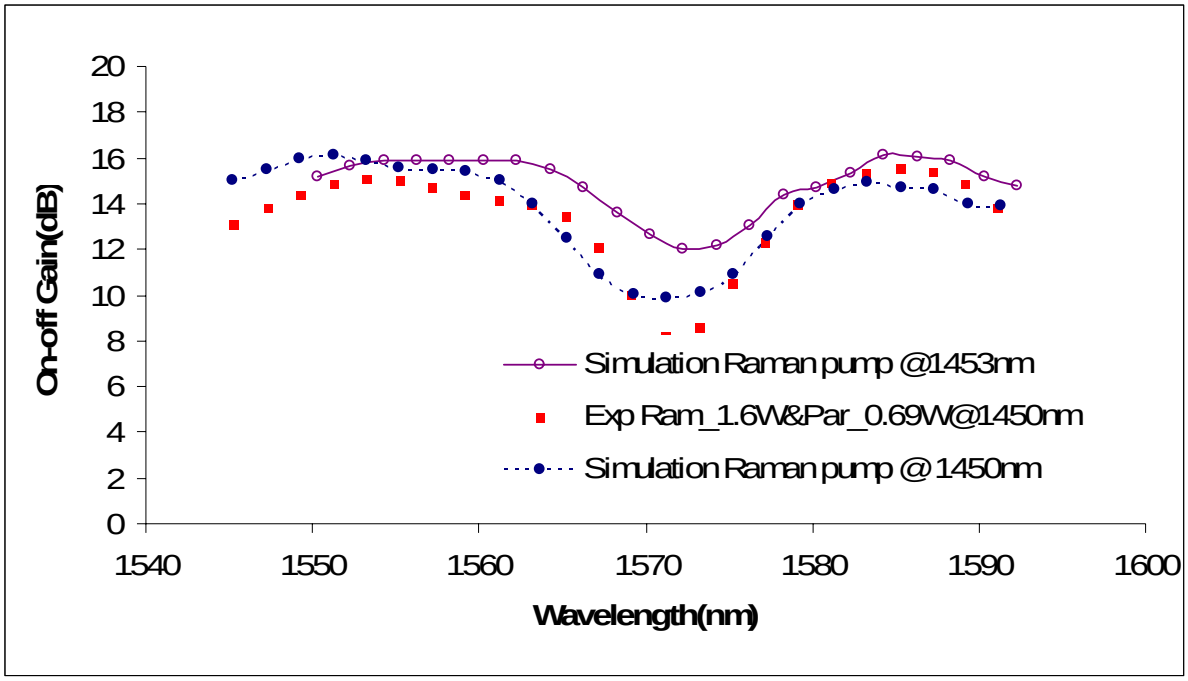


Fig.4.7.3. Tandem configuration: Gain curves showing the optimization of the gain flatness

### 4.7.2 Using two Raman pumps and a parametric pump

Similarly, a mathematical model was developed using two Raman pumps and a parametric pump. The aim was to observe the interaction between the Raman-Raman and Raman-parametric pumps and to see how this interaction affects the gain flatness and the bandwidth. We assumed that the ASE noise, Rayleigh scattering (RS) and pump depletion by the signals are neglected in the coupling equations. The mathematical model is divided into two parts. In part A, the interaction between the co-propagating

parametric pump and the two counter propagating Raman pumps was determined while, in part B, an expression for a net signal gain was established. In the following, the two parts are described in details.

**A. Analytical computation of the pump powers evolution**

In this section, an expression of pump power evolution for co-propagating parametric and two counter propagating Raman pumps is derived considering the pumps propagate alone (no presence of signal) but interacting with each other. The parametric pump wavelength was set at **1614 nm** while the Raman pumps were chosen to be at **1480 nm a**nd **1428 nm**. From the ASE profile to the Raman gain confirms that the interaction between the pumps (Raman-parametric) is due to the Raman effect, since the parametric pump lies in the gain region of both the Raman pump. Hence, it can be represented by the following coupling equations which ignore spontaneous Raman scattering, Rayleigh backscattering, higher-order Stokes waves and other nonlinear processes:

$$\frac{dP_P}{dz} = \frac{g_{\lambda R1}}{A_{eff}} P_{R1} P_{R2} P_P + \frac{g_{\lambda R2}}{A_{eff}} P_{R2} P_p - \alpha_P P_P \qquad (4.7.13)$$

$$\frac{dP_{R1}}{dz^*} = -\frac{\omega_{R1}}{\omega_P A_{eff}} g_{\lambda R1} P_p P_{R1} - \frac{\omega_{R1}}{A_{eff}\omega_{R2}} g_{\lambda R1} P_{R1} P_{R2} - \alpha_{R1} P_{R1} \qquad (4.7.14)$$

$$\frac{dP_{R2}}{dz*} = -\frac{\omega_{R2}}{\omega_p A_{eff}} g_{\lambda R2} P_{R2} P_P - \frac{\omega_{R2}}{\omega_{R1} A_{eff}} g_{\lambda R2} P_{R1} P_{R2} - \alpha_{R2} P_{R2} \qquad (4.7.15)$$

where $A_{eff}$ is the effective mode area of $P_{R1}, P_{R2}$ and $P_P$ are the Raman and parametric pump powers, $\omega_{R1,}$ $\omega_2$ and $\omega_P$ are the Raman and parametric pump frequencies, $\alpha_{R1,}$ $\alpha_{R2}$ and $\alpha_P$ are the attenuation coefficients of the Raman pump and parametric pump,

respectively. We will assume $z^*$ = L-z (where L is the fiber length and z is the propagation distance), since the Raman pump is counter propagating. The gain parameter $g_{\lambda R}$ is calculated from the ASE measurements. Note that Eqs. (4.7.13)-(4.7.15) assume a depolarized Raman pump.

Using the initial conditions, $P_P$(L=0Km) =0.25W, $P_{R1}$(L=0.5Km)=1.0W and $P_{R1}$(L=0.5Km)=1.2W and assuming that the Raman pump depletes, the approximate solution of Eqs. (4.7.13)-(4.7.15) can be obtained by dividing the total length of the fiber into small sections, each with length $\delta z$, and within each segment the light power can be considered to be constant. After iteration using the fourth order Runge-Kutta method, we can get the output power of the Raman and parametric pumps in each individual segment.

**B. Analytical computation of net gain**

Since the power of Raman and parametric pumps is known in every small segment $\delta z$, we calculate the signal gain due to the Raman pumps, $g_{R1}(\lambda, \delta z)$, $g_{R2}(\lambda, \delta z)$ and parametric pump, $g_p(\lambda, \delta z)$ for any segment. Hence, the net gain for the entire length (L) of the fiber due to Raman pump only, $g_{R1}(\lambda, L)$ and $g_{R2}(\lambda, L)$ and the net gain due to parametric pump only $g_p(\lambda, L)$ can be expressed as follows:

$$g_{R1}(\lambda, L) = (g_{R1}(\lambda, \delta z_1) g_{R1}(\lambda, \delta z_2) ..... g_{R1}(\lambda, \delta z_n)) \quad (4.7.16)$$

$$g_{R2}(\lambda, L) = (g_{R2}(\lambda, \delta z_1) g_{R2}(\lambda, \delta z_2) ..... g_{R2}(\lambda, \delta z_n)) \quad (4.7.17)$$

$$g_P(\lambda, L) = (g_P(\lambda, \delta z_1) g_P(\lambda, \delta z_2) ..... g_P(\lambda, \delta z_n)) \quad (4.7.18)$$

where $g_{R1}(\lambda,\delta z)$, $g_{R2}(\lambda,\delta z)$ and $g_P(\lambda,\delta z)$ are Raman and parametric gain in each segment

**a) Calculation of Raman gain for each segment, $g_{R1}(\lambda,\delta z)$ and $g_{R2}(\lambda,\delta z)$**

In order to calculate the Raman gain of individual segment $g_{R1}(\lambda,\delta z)$, we will approach by using a small-signal model and will assume the Raman pump to be constant within that segment. In the small-signal regime where pump depletion due to signal λ, is neglected, the evolution of the signal and the pump power level may be derived from Eqs. (4.7.1)-(4.7.2). and can be written as follows:

$$\frac{dP_s}{dz} = \frac{g_{\lambda R_i}}{A_{eff}} P_{R_i} P_s - \alpha_s P_s \tag{4.7.19}$$

$$\frac{dP_R}{dz^*} = -\alpha_{R_i} P_{R_i} \tag{4.7.20}$$

where $P_s$ is the signal power and $g_{\lambda Ri}$ is Raman gain coefficient and i=1 and 2. Note the first term of the Eq(4.7.2) is dropped in Eq(4.7.6) due to the assumption of non-depleted Raman pump. The solution for the small signal gain within the length, $\delta z$ can be derived by solving the coupling equations Eq(4.7.19) and Eq(4.7.20) analytically and can be expressed as follows:

$$g_{R1}(\lambda,\delta z) = EXP\left( g_{R1} \frac{P_{R1}(\delta z)}{A_{eff}\,\alpha_{R1}} \left(e^{\alpha_{R1}\delta z} - 1\right) - \alpha_s \delta z \right) \tag{4.7.21}$$

$$g_{R2}(\lambda, \delta z) = EXP\left( g_{R2} \frac{P_{R2}(\delta z)}{A_{eff}\,\alpha_{R2}} \left(e^{\alpha_{R2}\delta z} - 1\right) - \alpha_s \delta z \right) \qquad (4.7.22)$$

where $P_{R(\delta z)}$ Raman pump power within the small segment , $\delta z$ .

**b) Calculation of parametric gain within the segment,** $\delta z$

Similarly, we will find parametric amplification within the infinitely small fiber segment, $\delta z$ by considering strength of strong parametric pump ( $P_P(dz)$ ) be constant within the fiber segment, $\delta z$ and co-propagating with a signal $\lambda$, in the fiber with nonlinear coefficient γ (we assume that γ > 0, as in the case of silica fiber). Small signal theory reveals the existence of parametric gain, which amplifies the signal, as well as an idler arising at $\omega_i = 2\omega_p + \omega_s$ Amplification can be studied by means of the signal power gain in the length $\delta z$ of the fiber, given by:

$$g_P(\lambda, \delta z) = 1 + \left[ \frac{\gamma P_p(\delta z)}{g} \sinh(g \delta z) \right]^2 \qquad (4.7.23)$$

The parametric gain g is given by :

$$g^2 = -\Delta k_0 (\frac{\Delta k_0}{4} + \gamma P(\delta z)) \qquad (4.7.24)$$

where $\Delta k_0$ is the linear phase mismatch, which is expressed as:

$$\Delta k_0 = -\frac{2\pi c}{\lambda_0^2}\frac{dD}{d\lambda}(\lambda_p - \lambda_0)(\lambda_p - \lambda_s)^2 \qquad (4.7.25)$$

where $\lambda_p$ and $\lambda_s$ are the pump and signal wavelengths, respectively, $\lambda_0$ is the fiber's zero-dispersion wavelength, D is the chromatic dispersion.

Therefore, the total signal gain, $G_T(\lambda, L)$ (dB) due the Raman and parametric pump for the entire length, L is calculated by summing Eqs (4.7.21) and (4.7.22) and (4.7.23) and can be expressed as:

$$G_T(\lambda, L) = 10\log(g_{R1}(\lambda, L)) + 10\log(g_{R2}(\lambda, L) + 10\log(g_P(\lambda, L) \qquad (4.7.26)$$

And finally, the on/off gain is calculated by subtracting the total component losses ($L_T$ ) from the overall signal gain expressed by Eq. (4.7.26)

$$G_{(on/iff)} = G_T(\lambda, L) - L_T \qquad (4.7.27)$$

A computer model described above is used to optimize the gain flatness. The model shows that if the parametric pump wavelength is set at **1614 nm,** while the Raman pumps are tuned to **1428 nm a**nd **1480 nm,** more than 100nm of bandwidth with gain fluctuation of about 5dB can be achieved, as shown in Fig. 4.7.4. The model predicts that the

parametric pump power requires only 0.25 W compare to the Raman pumps power ($\approx 1.2W$) to obtain a gain of $14 \pm 5$ dB.

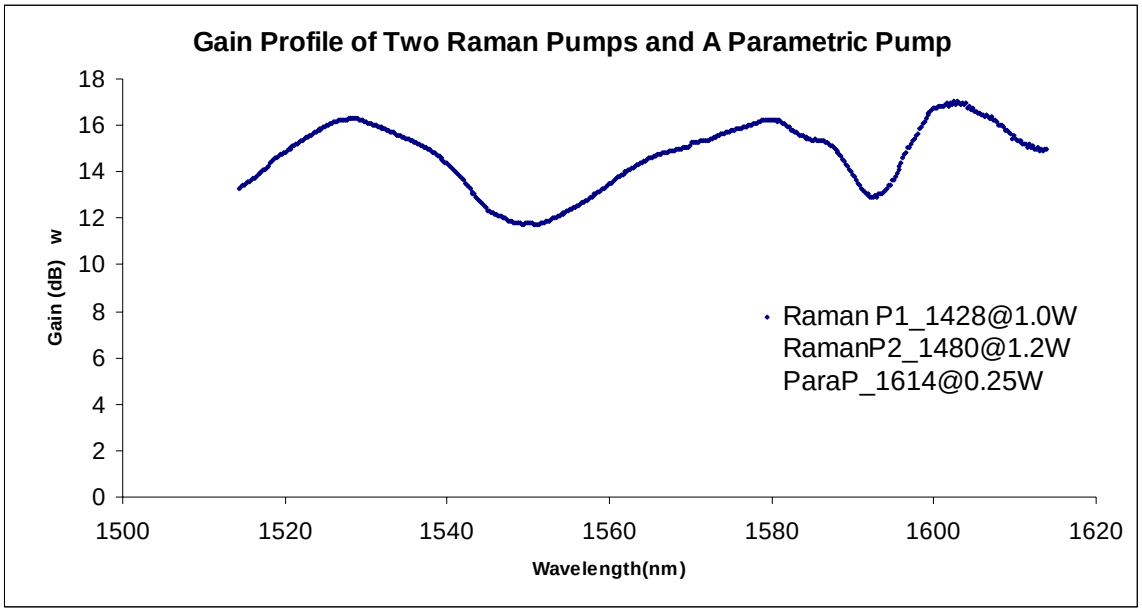


Fig.4.7.4. Unison configuration: Gain curves showing the optimization of the gain flatness

## 4.7.3 Conclusion

The model predicts that by combining two Raman and a parametric pump, we can achieve a bandwidth more than 100nm. From the simulation results, we conclude that in order the achieve flat gain, the pump powers must be adjusted in such a way that the depleted pumps (Raman pumps) must be set at high power levels while the amplified pump( parametric) must me kept at minimum power level. By cascading more units of the above combination of Raman and parametric pumps, it is possible to achieve the entire bandwidth of the optical communication spectrum.

# 5. Phase Characterization

## 5.1 Fundamentals of Semiconductor Optical Amplifier

There has been rapid growth in the deployment and capacity of optical fiber communication networks over the past twenty-five years. This growth has been made possible by the development of new optoelectronic technologies that can be utilized to exploit the enormous

bandwidth of optical fiber. Today, systems are operated at bit rates in excess of 100 Gb/s. Optical technology is the dominant carrier of global information. It is also central to the realization of future networks that will have the capabilities demanded by society. These capabilities include virtually unlimited bandwidth to carry communication services of almost any kind, and full transparency that allows terminal upgrades in capacity and flexible routing of channels. Many of the advances in optical networks have been made possible by the optical amplifier such as a Semiconductor Optical Amplifier (SOA).

An SOA uses the principle of stimulated emission to amplify an optical information signal. An optical input signal enters the semiconductor's active region through coupling optics. Injection current delivers the external energy necessary to pump electrons at the conduction band. The input signal stimulates the transition of electrons down to the valence band and the emission of photons with the same energy. The two basic SOA

types are the Fabry-Perot amplifier (FPA) and the traveling-wave amplifier which are shown in figure 5.1.1 and 5.1.2 respectively.

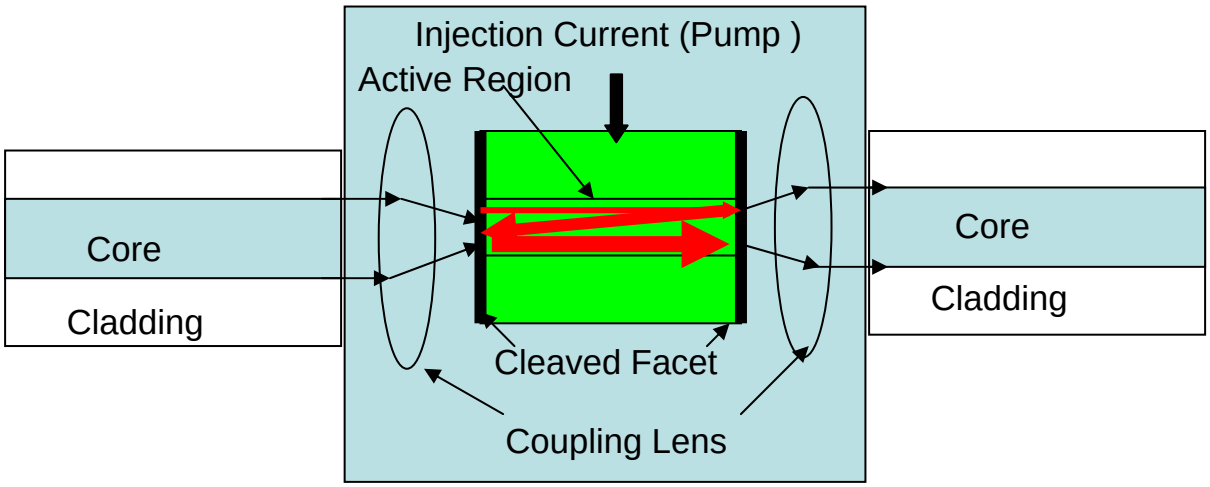


Fig.5.1.1 Fabry-Perot amplifier[41]

The FPA has the same configuration as a Fabry-Perot Laser. Light entering the active region is reflected several times from the cleaved facets before it leaves the active region. The gain of the FPA is represented by the equation 5.1.1 [41]

$$G_{FPA} = \frac{P_{out}}{P_{in}}$$

$$G_{FPA} = \frac{G_s(1-R)^2}{\left\{(1-RG_s)^2 + 4RG_s Sin^2\left[(\omega-\omega_0)\frac{L}{v}\right]\right\}} \qquad (5.1.1)$$

where $G_s$ is the single pass power amplification factor, $\nu$ is the speed of light within the cavity, R is the power reflection coefficient of the cleaved facets, L is the active region, w is the operating frequency and w0 is the central frequency. FPA gain is frequency dependent, which reaches its maximum at the central frequency. If we consider reflection occurring at the semiconductor –air interface, which is equal to 0.32, we will see that the single pass power amplification factor is less than 3.125.

$$G_{FPA} = \frac{G_s(1-R)^2}{(1-RG_s)^2}$$

$$1 - RG_s > 0$$
$$RG_s < 1$$
$$G_s < \frac{1}{R}$$
$$R = 0.32$$
$$G_s < 3.125$$

A Traveling wave amplifier is essentially an active medium without reflective facets so that an input signal is amplified by a single passage through the active region as shown below. Thus the gain of a TWA is the gain of an FPA with R=0 as given by the formula 5.1.2

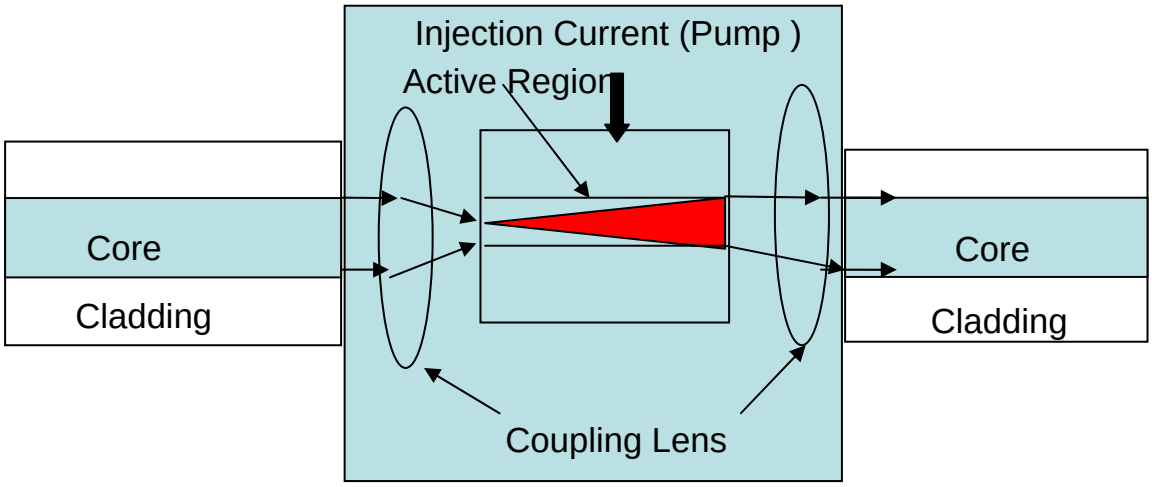


5.1.2 A traveling wave amplifier[41]

$$G_{TWA} = \frac{P_{out}}{P_{in}}$$

$$G_{TWA} = \frac{G_s (1-R)^2}{\left\{ (1-RG_s)^2 + 4RG_s Sin^2 \left[ (\omega - \omega_0) \frac{L}{v} \right] \right\}}$$

0 0 0

$$G_{TWA} = G_s \qquad (5.1.2)$$

## 5.2 Introduction and motivation

Semiconductor optical amplifiers (SOAs) have been extensively used in making optical switches, wavelength conversion devices [25], threshold devices and many other optical applications [26-29]. Optical logic gate operations were also performed by using a SOA placed in an asymmetric Mach-Zehnder interferometer. These devices exploit the ultra-fast *nonlinearities* of the SOA and the *phase change*, that occur when the signal passes through the SOA [30-32]. A number of experiments and models pertaining to the nonlinear behavior of SOAs including the gain dynamics and nonlinear polarization rotation have been previously conducted [33-34]. Pump-probe methods to measure the time resolved gain and phase dynamics [35-36], and recently, a method based on a Sagnac fiber loop was employed to measure the linewidth enhancement factor [37].

In this thesis, we demonstrate an experimental methodology to characterize the phase as a function of input power to the SOA. The principle of the method is divided into two steps. Firstly, the phase difference is expressed between two pulses (clockwise and counter clockwise) in an asymmetric Sagnac interferometer as a function of input intensity. The clockwise pulse is attenuated so that the SOA gain remains linear throughout the input intensity variation while the counterclockwise pulse exhibits a non-linear gain response at a higher input power. Secondly, the phase difference function is separated into a linear and a nonlinear region, and by using the initial boundary

conditions, an expression for a phase as a function of input intensity to the SOA is determined.

This is carried out at three different gain levels by setting the drive current of the SOA to 170mA, 190mA and 200mA.

# 5.3 Experimental Technique

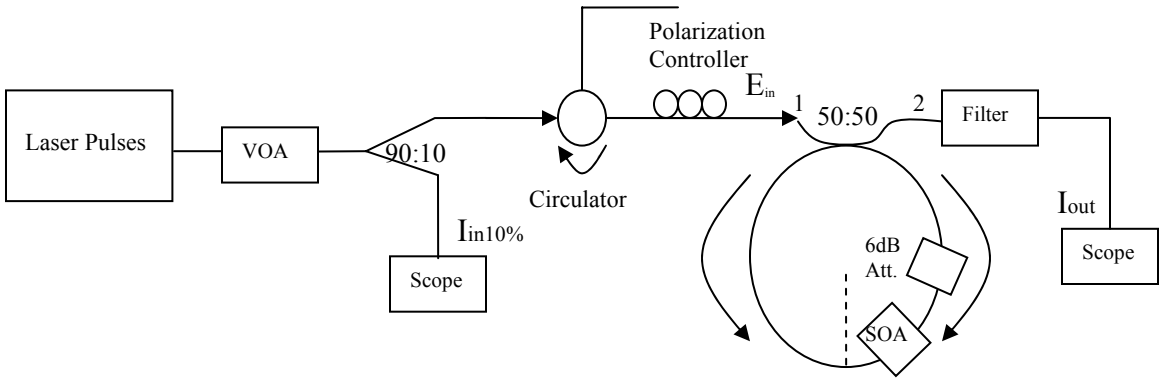


Fig.5.3.1. Experimental setup

The setup is presented in Fig.1. The device consists of an optical attenuator, a commercial SOA (InPhenix model IPSAD 1501) having 18dB of small signal gain and a 2x2 symmetric directional coupler with good uniformity (0.3dB); low excess loss (<0.1dB), and very low polarization dependent loss (<0.1dB). One of the ports of the 2x2 coupler is used as the input terminal and another port is used as the output terminal. The other two terminals of the coupler are connected to a 5m long section of standard single mode fiber in a loop mirror configuration which includes the SOA and the attenuator.

A continuous-wave (CW) laser tuned at 1550nm was externally modulated to generate 100 picoseconds pulses at a 78 MHz repetition rate. These pulses were

channeled into a variable optical attenuator (VOA), and then to a 90:10 coupler. The 90:10 coupler has similar uniformity, excess loss, and polarization loss as the symmetric coupler. The 90% output port was connected to either an isolator (not shown) or a circulator, while the 10% port of the coupler was used to monitor the input power (i.e., $I_{in10\%}$). Both the circulator and the isolator prevent light from returning to the modulator, however, the circulator also allowed us to monitor reflected light from the loop mirror. The VOA was used to control the power that entered the loop mirror, while the drive current of the SOA controlled the gain and was set to 170, 190 and 200mA. The loop attenuator was kept constant at 6dB. A bandpass filter was used to filter out the broadband emission from the SOA. The output of the device was measured with a sampling oscilloscope.

In order to collect a lot of data and reduce the measurement error, we automated the acquisition system. The software that incremented the attenuation of the VOA by 0.5dB per step controlled the input intensity to the loop mirror. The signal analyzer was set to average the peak intensity of 20 data pulses to provide a single data point. The standard deviation over the 20 data pulses was observed to be less than 1%.

To make sure that the output of a balanced loop mirror with an attenuator was independent of the input intensity, we devised the following setup as shown in figure 5.3.2. We took the SOA out of the setup and the output of the loop mirror was minimized by adjusting the Polarization controller. We noticed that the output of the loop mirror

remained the same even though the input intensity was varied by the VOA as shown in figure 5.3.2

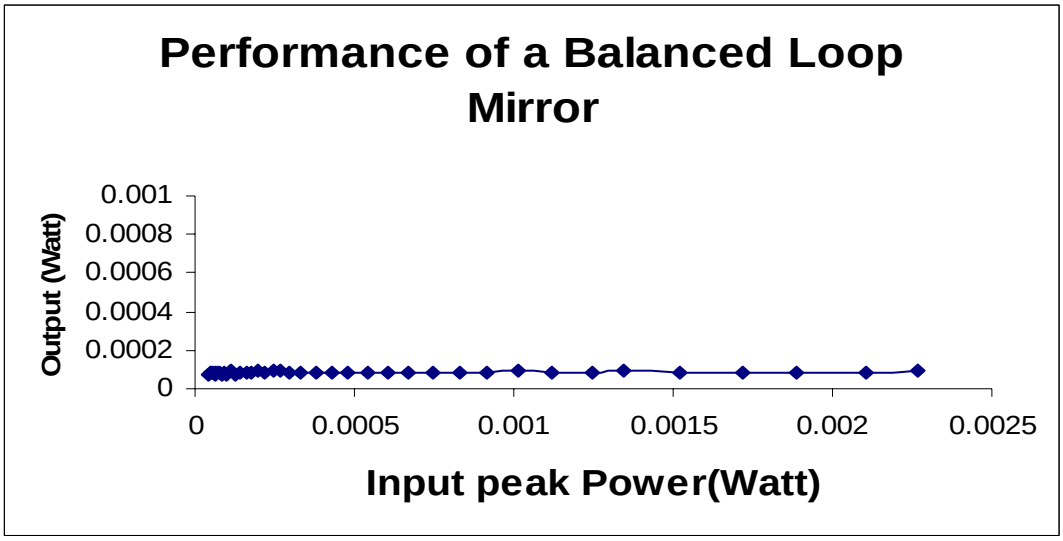


Fig.5.3.2 The output of the balanced loop mirror remained constant throughout the experiment

# 5.4. Concept of Method

5.4.1. *Derivation of phase difference as a function of input intensity*

We have developed a simple model to describe the experimental results and to gain information about the nonlinear phase response of the SOA. When an input pulse $E_{in} = A_{in}e^{i\theta_{in}}$, as shown in Fig.1, enters the 50:50 coupler, it is split into two pulses propagating clockwise and counter clockwise. The pulse that propagates in the counter-clockwise direction encounters amplification first and then attenuation, while the other that propagates in the clockwise direction undergoes attenuation first and then amplification. The electric field at the output port $E_t$ can be written as:

$$E_t = A_c e^{i(\theta_{in}+\delta_c+\pi)} + A_{cc} e^{i(\theta_{in}+\delta_{cc})} \qquad (5.4.1)$$

where $A_c$ and $A_{cc}$ are the amplitudes of the clockwise and counter clockwise propagating electromagnetic fields respectively. The two pulses undergo phase shifts while propagating through the SOA. However, the phase shifts, $\delta_c$ and $\delta_{cc}$ are different since the input intensities are different in each direction, assuming no pulse overlap. To insure that there is no pulse overlap, the SOA is located asymmetrically within the loop, offset a propagation distance that is longer than the pulse length in the fiber (we also offset the

SOA an additional amount to account for the gain recovery time). A sufficiently low repetition rate of 78MHz is used allowing us to ignore gain recovery dynamics.

$A_c$ and $A_{cc}$ in equation (1) can be expressed as follows:

$$A_c = \sqrt{I_c \alpha_c} \tag{5.4.2}$$

$$A_{cc} = \sqrt{I_{cc} \alpha_{cc}} \tag{5.4.3}$$

where $\alpha_c$ and $\alpha_{cc}$ are the coupling ratios and $I_{cc}$ and $I_c$ are the peak intensities measured at two different locations, as shown in Fig. 5.4.1(b) and Fig.5.4.1(c).

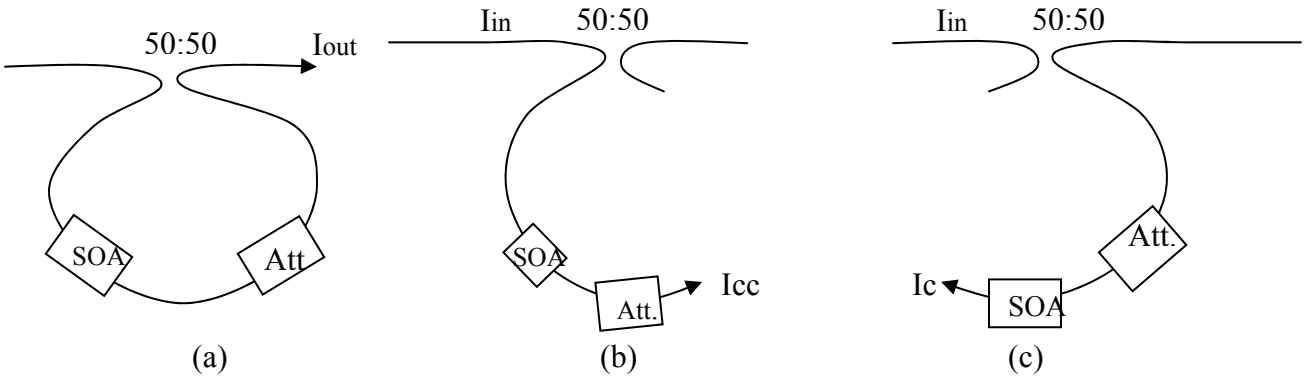


Fig.5.4.1 Description of the experimental configurations used to measure the nonlinear response functions of the loop mirror and the gain saturation of the SOA. a) Iout is defined as the output of the loop mirror b) Icc is defined as the signal which is amplified first and then attenuated. c) Ic is defined as the signal which is attenuated first and then amplified.

$I_{cc}$ is the peak counter-clockwise intensity that is recorded after the signal encounters amplification and then attenuation. As the signal intensity is slowly increased by varying the VOA, the gain of the SOA shifts from the linear to the saturation region. However, $I_c$ is the peak clockwise intensity that is recorded after the signal first undergoes attenuation and then amplification. The signal intensity is significantly reduced by the attenuator before it encounters the SOA. Therefore, this signal remains in the linear gain region of the SOA for the entire scan as shown in Fig. 5.4.2.

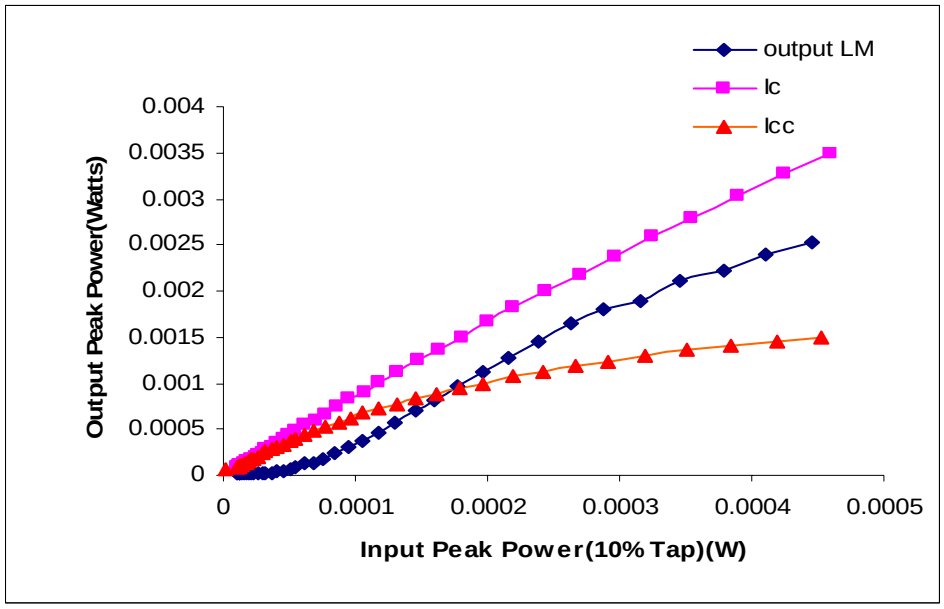


Fig.5.4.2 Peak intensities $I_{out}$, $I_{cc}$, $I_c$ as a function of input power

Substituting equations (2) and (3) into (1), the resultant electric field at the output of the loop mirror can be expressed as follows:

$$E_t = \sqrt{I_c \alpha_c} e^{i(\theta_{in} + \delta_c + \pi)} + \sqrt{I_{cc} \alpha_{cc}} e^{i(\theta_{in} + \delta_{cc})} \tag{5.4.4}$$

The product of the resultant electric field $E_t$ and its conjugate $E_t^*$ can be used to get the output intensity $I_{out}$ :

$$I_{out} = E_t E_t^*$$

$$I_{out} = I_c \alpha_c + I_{cc} \alpha_{cc} - 2\sqrt{I_c I_{cc} \alpha_c \alpha_{cc}} \cos(\delta_{cc} - \delta_c) \tag{5.4.5}$$

Solving the above equation for the phase difference $\delta_{cc} - \delta_c$ :

$$\delta_{cc} - \delta_c = \cos^{-1}\left( \frac{I_c \alpha_c + I_{cc} \alpha_{cc} - I_{out}}{2\sqrt{\alpha_c \alpha_{cc} I_c I_{cc}}} \right) \tag{5.4.6}$$

Therefore, the phase difference for each data point can be numerically calculated from the intensities $I_c, I_{cc}, I_{out}$ and the coupling ratios. Fig.5.4.3 shows the phase difference plotted as a function of the input intensity ($I_{in10\%}$). The solid line in Fig. 5.4.3 is a fit to the experimental data using a third order polynomial:

$$\delta_{cc} - \delta_c = \Delta\theta = a I_{in10\%}^3 + b I_{in10\%}^2 + c I_{in10\%} + d \tag{5.4.7}$$

The goodness of fit expressed by the correlation coefficient $r^2 = 0.9987$ is also given in Fig. 5.4.3. The coefficients *a*, *b*, *c* and *d* in equation (5.4.7) were obtained from the fitting. The values of the coefficients *a*, *b*, *c* and *d* for different SOA gain settings can be

used to determine the actual phase δ as a function of input intensity. The procedure is outlined below.

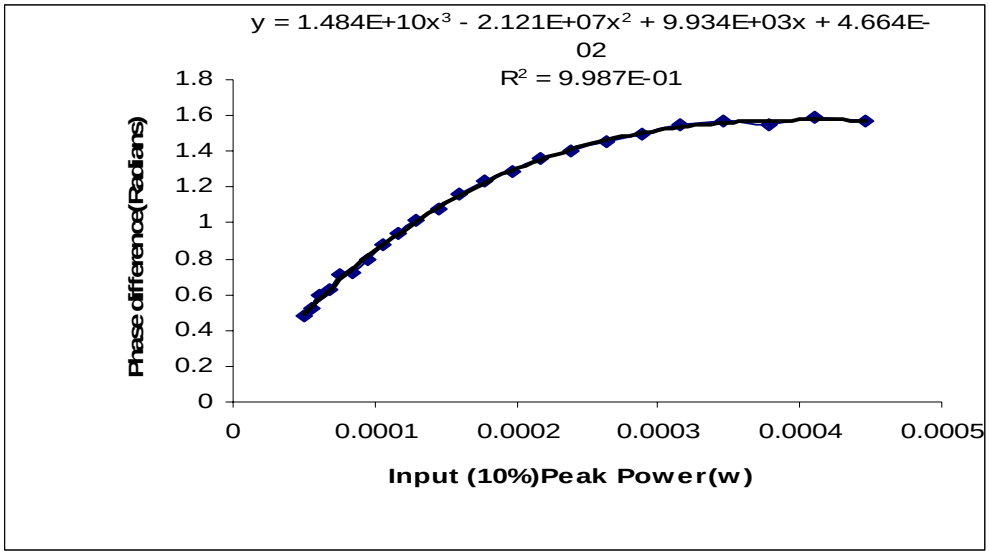


Fig.5.4.3 Phase difference as function of Input power (measured at the 10% tap port). The solid line is the fit using a third order polynomial

5.4.2. *Derivation of Phase as a function of input intensity to the SOA in the Linear Region*

The phase difference, Δθ has two operating regions - a linear region where the phase difference is $\Delta\theta_L$ and a non-linear region where the phase difference is $\Delta\theta_{NL}$. Focusing just on the linear part of equation (5.4.7), a relationship between input intensity to the SOA and the phase can be established. We will now assume that $I_{(SOA)c}$ and $I_{(SOA)cc}$ are clockwise and counter clockwise peak intensities entering the SOA from both

directions respectively. When the intensities in both directions are low, the gain of the SOA remains in the linear region, as does the phase difference Δθ. If the phase difference is linear then we can assume that the phase is also linear in each direction. Equation (5.4.7) has an offset of *d,* which is due to the amplified spontaneous emission (ASE) of the SOA and the signal noise. We can neglect the offset by introducing zero initial conditions, i.e.

$$I_{(SOA)cc} = I_{(SOA)c} = 0; d = 0$$

Using the linear term of equation (5.4.7), the linear phase difference can be expressed as:

$$\Delta\theta_L = cI_{(in10\%)} \tag{5.4.8}$$

Since $\delta_c$ and $\delta_{cc}$ are in the linear region, they are expressed as a product of input intensity and a slope, K

$$\delta_{cc} = KI_{(SOA)cc} \tag{5.4.9}$$

$$\delta_c = KI_{(SOA)c} \tag{5.4.10}$$

$$\delta_{cc} - \delta_c = \Delta\theta_L \tag{5.4.11}$$

Replacing $\delta_c$ and $\delta_{cc}$ by equations (5.4.9) and (5.4.10)

$$KI_{(SOA)cc} - KI_{(SOA)c} = \Delta\theta_L \tag{5.4.12}$$

Factorizing K and substituting equation (5.4.8) for $\Delta\theta_L$, equation (5.4.12) can be written as

$$K = \frac{cI_{in10\%}}{(I_{(SOA)cc} - I_{(SOA)c})} \tag{5.4.13}$$

Since $I_{(SOA)c}$ and $I_{(SOA)cc}$ are the input intensities into the SOA's clockwise and counter clockwise directions respectively, they can be expressed as a function of $I_{in10\%}$ and attenuation factors, $\beta_c$ and $\beta_{cc}$. The attenuation factors (clockwise) $\beta_c$ and (counterclockwise) $\beta_{cc}$ were measured as 1.03 and 5.89 respectively and $I_{(SOA)c} = \gamma I_{(SOA)cc}$ where $\gamma = \frac{\beta_c}{\beta_{cc}}$, resulting in the following expression for K

$$K = \frac{cI_{10\%}}{(\beta_{cc} - \beta_c)I_{10\%}} \tag{5.4.14}$$

Using the value of K in equations (5.4.9) and (5.4.10), the linear phase can be expressed as a function of SOA input intensity.

$$\delta_c = \frac{c}{(\beta_{cc} - \beta_c)} I_{(SOA)c} \tag{5.4.15}$$

$$\delta_{cc} = \frac{c}{(\beta_{cc} - \beta_c)} I_{(SOA)cc} \tag{5.4.16}$$

5.4.3. *Derivation of Phase as a function of input intensity to the SOA in the Nonlinear Region*

Similarly, using the non-linear part of the equation (5.4.7), the non-linear phase difference $\Delta\theta_{NL}$ can be expressed as follows:

$$\Delta\theta_{NL} = aI_{in10\%}^3 + bI_{in10\%}^2 \tag{5.4.17}$$

From Fig. 5.4.3 one can see that $I_{(SOA)c}$ remained in the linear region throughout the experiment while $I_{(SOA)cc}$ moved to the non-linear region. Thus $\delta_c$ can still be expressed as equation (5.4.15):

$$\delta_{cc} - \delta_c = \Delta\theta_{NL}$$

$$\delta_{cc} = \Delta\theta_{NL} + \delta_c$$

$$\delta_{cc} = aI_{in10\%}^3 + bI_{in10\%}^2 + \frac{c}{(\beta_{cc} - \beta_c)} I_{(SOA)c} \tag{5.4.18}$$

$I_{in10\%}$ and $I_{(SOA)c}$ can be expressed in terms of $I_{(SOA)cc}$ by using attenuation factor $\beta_{cc}$ in equation (5.4.18). $\delta_{cc}$ be finally expressed as a function of input intensity to the SOA by the equation below:

$$\delta_{cc} = \frac{a}{\beta_{cc}^3} I_{(SOA)cc}^3 + \frac{b}{\beta_{cc}^2} I_{(SOA)cc}^2 + \frac{\gamma c}{(\beta_{cc} - \beta_c)} I_{(SOA)cc} \tag{5.4.19}$$

## 5.5 Discussion

The constants a, b, and c are the coefficients from the third order polynomial, as shown in Fig. 5.4.3, while $\beta_c$, $\beta_{cc}$ and $\gamma$ are the measured attenuation factors, as shown in the table below.

| Constants | $a$ | $b$ | $c$ | $\gamma$ | $\beta_c$ | $\beta_{cc}$ |
|---|---|---|---|---|---|---|
| Gain @ 200mA | 1.484E+10 | -2.121E+7 | 9.934E+3 | 0.17 | 1.03 | 5.89 |
| Gain @ 190mA | 1.243E+10 | -1.735E+7 | 8.101E+3 | 0.17 | 1.03 | 5.89 |
| Gain @ 170mA | 1.73E+10 | -6.864E+6 | 5.585E+3 | 0.17 | 1.03 | 5.89 |

Each one of these coefficients is substituted in the equation (5.4.19). Three equations for three different gain levels are obtained. Fig. 5.4.4 is a plot of these equations.

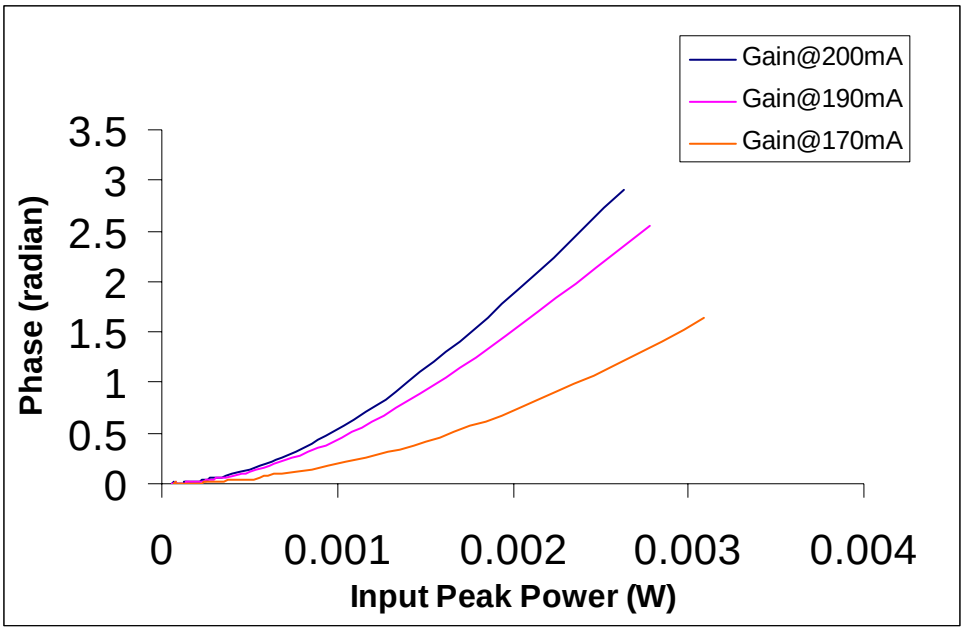


Fig.5.4.4. Nonlinear phase as a function of input peak intensity into the SOA at two different bias current levels

It represents the relationship between the phase and the input intensity to the SOA. At low input power it is noticed that the signal undergoes very small phase change, irrespective of the gain setting. However, as the power increases the curves begin to diverge. It is observed that for values of the input signal power beyond 0.001 W, the slopes of the curves become steeper as the gain of the SOA increases. This implies that in order to achieve a large phase shift at low input signal power, the gain level of the SOA must be set to a higher value. While we showed above that the noise in the measurement was less than 1% we wanted to verify the reproducibility of our measurements. To do this, multiple measurements for the same input condition were taken over a period of several days.

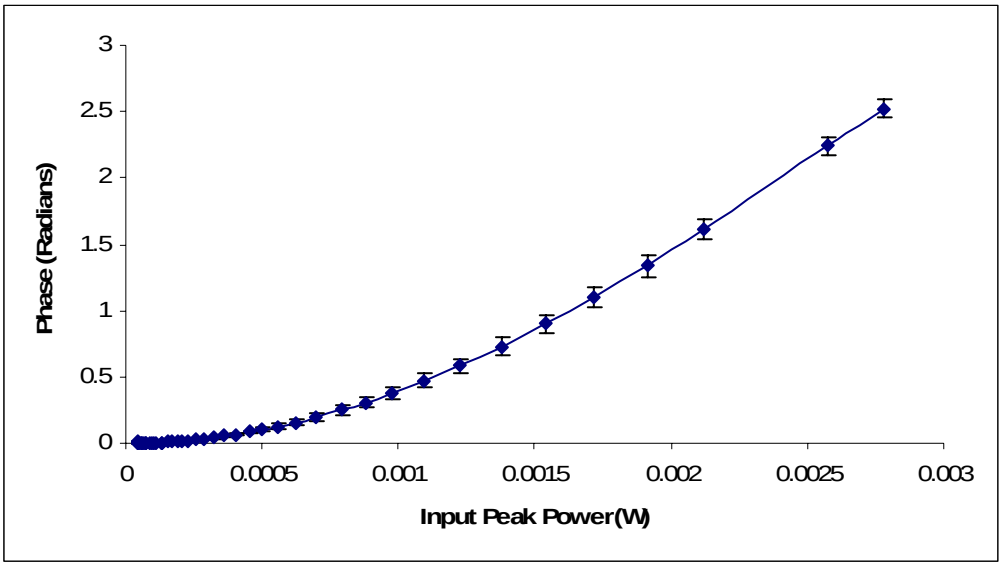


Fig. 5.4.5 Mean Nonlinear Phase between experiments and their variability over different days. Variability ranges from 16% at low input power to less than 3% at high input power

We find the variability between these experiments to range from 16% at low input power to less than 3% at high input power (See Fig. 5.4.5). These uncertainties compare favorably to the difference of the measurement under various conditions tested showing the reproducibility of the experiment.

We have presented an experimental methodology to characterize the phase as a function of input power to the SOA. The counter clockwise and clockwise pulses, which propagate mutually in the opposite directions, travel the same distance through the same media. Therefore, we are able to eliminate the phase measurement errors due to environmentally dependent path lengths.

# Chapter 6

**Conclusion and Future work**

In this dissertation, we have investigated two different nonlinear processes in a distributed medium, such as, a highly non-linear fiber (HNLF) and have demonstrated that by combining optical fiber parametric amplification with Raman fiber amplification, we could further extend the flat gain bandwidth of a Raman fiber amplifier. The parametric process enabled an increase in gain bandwidth by extending the gain region to the longer wavelength side of the Raman gain. Two different configurations of the amplifier were investigated, and their gains and bit error performances were characterized. We have also developed a model that predicts if two Raman and a parametric pump are combined in a unison configuration, we can achieve a bandwidth more than 100nm. From the simulation results, we conclude that in order the achieve flat gain, the pump powers must be adjusted in such a way that the depleted pumps (Raman pumps) must be set at high power levels while the amplified pump( parametric) must me kept at minimum power level. By cascading more units of the above combination of Raman and parametric pumps, it can be possible to achieve the entire bandwidth of the optical communication spectrum.

We also developed an experimental methodology to characterize the phase as a function of input power to the Semiconductor Optical Amplifier (SOA).This was carried out at three different gain levels by setting the drive current of the SOA to 170mA, 190mA and 200mA. This characterization could be used to develop switches and gates.

## REFERENCES


[1] S. Namiki and Y. Emori, "Ultra broad-band Raman amplifiers pumped and gain equalized by wavelength division multiplexed high power laser diodes," IEEE J. Selec. Topics in Quant. Elec., 7 (1), pp 3-16 (2001)

[2] T.N. Nielsen et al., Proc. Opt. Fiber Commun. Conf. 4 (2000) 236.

[3]. L.D. Garrett, M. Eiselt, R.W. Tkach, V. Dominic, R. Waarts, D. Giltner, D. Mehuys, IEEE Photon. Technol. Lett. 13 (2001) 157

[4] S. Namiki, Y. Emori, IEEE J. Sel. Top. Quantum Electron. 7 (2001) 3.

[5] S.H. Chang, S.K. Kim, H.S. Chung, M.J. Chu, IEEE Photon. Technol. Lett. 15 (2003) 906.

[6] G. Cappellini and S. Trillo, "Third-order three-wave mixing in single mode fibers: Exact solutions and spatial instability effects," *J. Opt. Soc. Amer. B, Opt. Phys.*, vol. 8, no. 4, pp. 824–838, Apr. 1991.

[7] M. C. Ho, K. Uesaka, M. E. Marhic, Y. Akasaka, and L. G. Kazovsky,"200-nm-bandwidth fiber optical amplifier combining parametric and Raman gain," *J. Lightwave Technol.*, vol. 19, pp. 977–981, July 2001.

[8] J. Hansryd and P. A. Andrekson, "Broad-band continuous-wave-pumped fiber optical parametric amplifier with 49-dB gain and wavelength-conversion efficiency," *IEEE Photon. Technol. Lett.*, vol. 13, pp. 194–196, Mar. 2001

[9] Altuncu A., Siddiqui A.S., Ellis A., Newhouse M.A., Antos A.J. " Gain and noise figure characterization of a 68 km long distributed erbium doped fiber amplifier ",Electronics Letters, Vol.32, No.19, 1800-1801, 1996.

[10] H. S. Seo, Y. G. Choi, B. J. Park, D. H. Cho, and K. H. Kim, "Simultaneous amplification by Er-ions and SRS in a Er-doped germano-silica fiber," *IEEE Photon. Technol. Lett.*, vol. 15, no. 9, pp. 1198–1200, Sep. 2003.

[11] Y. Kurosawa, N. Takeda, T. Kawazawa, H. Taga, and K. Goto, "Raman assisted EDF amplifier using 1460 nm pump wavelength for C-band transmission with long repeater span," presented at the Eur. Conf. Optical Communication (ECOC), Rimini, Italy, Sep. 2003, Paper Tu3.2.5.

[12] Jian Chen, Xueming Liu, Chao Lu, "Design of Multistage Gain-Flattened Fiber Raman Amplifiers", Journal of Lightwave Technology, VOL. 24, NO. 2, FEBRUARY 2006

[13] E. Golovchenko, P. V. Mamyshev, A. N. Pilipetskii and E. M. Dianov, "Mutual influence of the parametric effects and stimulated Raman scattering in optical fibers," IEEE J. Quantum Electron. **26**, 1815-1820 (1990).

[14] A. S. Y. Hsieh, S. G. Murdoch, S. Coen, R. Leonhardt and J. D. Harvey, "Influence of Raman susceptibility on parametric amplification in optical fibers," Opt. Lett. **32**, 521-523 (2007)

[15] Joa˜o F.L. Freitas, M.B. Costa e Silva, S.R. Lu¨ thi, A.S.L. Gomes, "Raman enhanced parametric amplifier based S–C band wavelength converter: Experiment and simulations", Optics Communications 255 (2005) 314–318

[16] H. K. Y. Cheung, K. K. Y. Young, N. Wong and M. E. Marhic, "Gain optimization of Raman mediated fiber optical parametric amplifiers," paper 6103-28, SPIE Photonics West, 2006

[17] D. A. Chestnut, C. J. S. de Matos and J. R. Taylor, "Raman assisted fiber optic parametric amplifier and wavelength converter in highly nonlinear fiber," J. Opt. Soc. Am. B, 19 ( 8), pp. 1901 – 1904 (2002)

[18] J. F. L. Freitas, M.B. Costa e Silva, S.R. Luthi and A.S.L. Gomes, "Raman enhanced parametric amplifier based S-C based band wavelength converter: Experiment and simulations," Opt. Comm. 255, pp 314-318 (2005)

[19] Jinye Zhang and M. R. Phillips, "Modeling intensity noise caused by stimulated Brillouin scattering in optical fibers," accepted for
presentation at *Conference on Lasers and Electro-Optics 200*5, Paper CMH6 (2005)

[20] Eva Peral and Amnon Yariv, "Degradation of modulation and noise characteristics of semiconductor lasers after propagation in optical fiber
due to a phase shift induced by stimulated Brillouin scattering," *IEEE J. Quantum Electronic*s, Vol. 35, pp. 1185-95 (1999)

[21] M. Horowitz, A. R. Chraplyvy, R. W. Tkach, and J. L. Zyskind, "Broad-band transmitted intensity noise induced by Stokes and anti-Stokes Brillouin scattering in single-mode fibers," IEEE Phot. Tech. Lett., Vol. 9, pp. 124-6 (1997)

[22] N.M. Nguyen-Vo and S. J. Pfeifer, " A Model of Spontaneous Brillouin Scattering as the Noise Source for Stimulated Scattering" IEEE Journal of Quantum Electronics. Vol. 29. No. 2. February 1993

[23] P. Kylemark, P.-O. Hedekvist, H. Sunnerud, M. Karlsson, and P. A. Andrekson, "Noise characteristics of fiber optical parametric amplifiers," *J. Lightw. Technol.*, vol. 22, no. 2, pp. 409–416, Feb. 2004.

[24] A. Bogris, D. Syvridis, P. Kylemark, and P. A. Andrekson, "Noise characteristics of dual-pump fiber-optic parametric amplifiers," *J. Lightw. Technol.*, vol. 23, no. 9, pp. 2788–2795, Sep. 2005.

[25] C. Janz, B. Lavigne, F. Poingt, I. Guillemot, F. Gaborit, B. Dagens, D.Chiaroni, and M. Renaud, "Low-penalty 10 Gbit/s operation of polarization-insensitive Mach–Zehnder wavelength converters based on bulktensile active material," in *Tech. Dig. Opt. Fiber Comm. (OFC'98)*, SanJose, CA, Feb. 22–27, 1998, pp. 101–102.

[26] K. Stubkjaer, "Semiconductor optical amplifier-based all-optical gates for high-speed optical process", J. Select. Topics. in Quantum Electron., vol. 6, pp. 1428-1433, 2000.

[27] M. Eiselt," Optical loop mirror with semiconductor laser amplifier", Electron. Lett., vol 28, pp1505-1507, 1992.

[28] Masahiko Jinno and Takao Matsumoto, " Nonlinear Sagnac Interferometer Switch and its Applications", IEEE Journal Of Quantum Electronics, vol. 28, No. 4, April 1992.

[29] N. S. Patel, K. L. Hall, K. A. Rauschenbach: Optics Lett. **21** (1996) 1466

[30] M. Eiselt: Electron. Lett.**28** (1992) 1505

[31] J. P. Sokoloff, P. R. Prucnal, I. Glesk, M. Kane: A Terahertz Optical Asymmetric Demultiplexer (TOAD), OSA Proceedings on Photonics in Switching, (Eds. J. W. Goodman, R. C. Alferness) Optical Society of America, Washington, D.C. 1993 **1**6, PD-4; J. P. Sokoloff, P. R. Prucnal, I. Glesk, M. Kane:IEEE Photon. Technol. Lett. **5** (1993) 787

[32] Y. Liu; M.T. Hill; E. Tangdiongga; H. de Waardt; N. Calabretta; G.D. Khoe; H.J.S. Dorren, "Wavelength conversion using nonlinear polarization rotation in a single semiconductor optical amplifier" Photonics Technology Letters, IEEE Volume 15, Issue 1, Jan. 2003 Page(s):90 – 92

[33] E. A. Patent, J. J. G. M. van der Tol, J. J. M. Binsma, Y. S. Oei, E. A. J. M. Bente, and M. K. Smit, "Self-Switching in Mach–Zehnder Interferometers with SOA Phase Shifters" IEEE Photonics Technology Letters, Volume. 17, No. 11, November 2005

[34] Daisuke Miyashita, Xueliang Song, Zhenrui Zhang, Naoki Futakuchi, and Yoshiaki Nakano, Fabrication and characterization of soa and phase shifter Integrated interferometer All-optical switches by single-step GaInAsPAnP selective area Movpe" International

Conference on Indium Phosphide and Related Materials, Santa Barbara, California, May 12-16, 2003, IEEE Lasers & Electro Opt Soc; IEEE Electron Devices Soc

[35] K. Inoue and T. Mukai, " Signal wavelength dependence of gain saturation in a fiber optical parametric amplifier", Optics Letters, Volume 26, No. 1, January 1,2001

[36] John A. Buck "Fundamentals of Optical Fibers"(A John Wiley & Sons, Inc., Publication, ISBN 0-471-22191-0, 2004) 2nd Edn.

[37] Govind P. Agrawal "Nonlinear Fiber Optics"( Academic Press, ISBN13:978-0-12-369516-1) 4th Edn.

[38] Carlo G. Someda, *Electromagnetic Waves*, Chapman & Hall (1998)

[39] Guang S. He, Song H.Liu, "Physics of Nonlinear Optics"(World Scientific, ISBN98102-3319-1)

[40] R. W. Boyd, Nonlinear Optics (Academic Press, San Diego, 1992).

[41] Djafar Mynbaev, "Fiber-Optic Communications Technology"( Prentice Hall, ISBN: 9780139620690)

# Conference/Publications

1) Extending the flat gain bandwidth of combined Raman-parametric fiber amplifiers using highly nonlinear fiber. Arend, M. F.; **Ummy, M. A**., Leng, L. and Dorsinville, R. Nonlinear Frequency Generation and Conversion: Materials, Devices, and Applications VI. Edited by Powers, Peter E., Proceedings of the SPIE, Volume 6455, pp. 64550 (2007).
2) Measurement of Nonlinear Phase of a SOA using an Asymmetric Loop Mirror, **Muhammad Ali Ummy**; Mark Arend; Mohammad Ali; Roger Dorsinville (accepted in Optics and Laser Technology)
3) Extending the flat gain bandwidth of combined Raman-parametric fiber amplifiers using highly nonlinear fiber. **Muhammad Ali Ummy,** Arend, M. F.; Leng, L. and Dorsinville, R. (in preparation)